LUNAR ORBITER GRAVITY ANALYSIS

J. LORELL
Jet Propulsion Laboratory, California Institute of Technology, Pasadena, Calif., U.S.A.

(Received 26 August, 1969)

Abstract. This paper presents the results to date of the Jet Propulsion Laboratory (JPL) effort at analyzing the tracking data from the five Lunar Orbiter spacecraft. Emphasis is placed on the long-arc evaluation, to which most of the work was directed, rather than on the mascon analysis, which will be reported separately.

The model of the Moon's gravity field that has been derived from the long-arc analysis is interpreted in terms of the Moon's mass distribution. The results are evaluated from the point of view of consistency and of statistical significance. In particular, the various factors contributing to the uncertainty in the estimation process are discussed.

1. Introduction and Summary

On August 14, 1966, Lunar Orbiter I became the first NASA spacecraft to orbit the Moon*. During the next $1\frac{1}{2}$ years, four more orbiters were successfully put into orbit. The tracking data from these five spacecraft constitute a unique source of information on the Moon's gravity field [1]. Since at present there are no plans to launch additional orbiters for gravity studies (Apollo orbiters will not serve this purpose), this data will not soon be superseded. Therefore, it is important that the data be subjected to a careful and thorough analysis.

Gravity studies, initiated shortly after the first tracking data was received, are still continuing at JPL and at Langley Research Center (LaRC). NASA provided the funding as the Lunar Orbiter Selenodesy Experiment (cf. [1]). The results of these studies to date have given a good qualitative understanding of the Moon's gravity field. However, from a quantitative view, the outcome has been somewhat less than definitive.

The purpose of the present paper is to summarize and evaluate the JPL part of the Selenodesy Experiment after 2 years of activity. Work on the experiment has been separated into two phases, short-arc analysis and long-arc analysis. It was planned to estimate the global distortions of the gravity field, i.e., the low-order harmonics, by calculating the trends in the orbital elements over long-time periods, hence the term long-arc analysis. Then, the short-arc perturbations would yield high-order effects. Results, and the degree of success, are discussed in the following.

The tracking information consists of Doppler and ranging data from 24 arcs of the

* There have been two other lunar orbiters, Russia's Luna X, put in orbit on April 3, 1966 and tracked for 57 days, and NASA's Anchored IMP, launched in July of 1967. The data from Luna X has not been made available to the west, although a listing of the orbital elements, and a derived set of harmonics has been published [2]. The Anchored IMP had a very loose orbit (semi-major axis = 5980 km) which does not give strong information on the gravity field.

The Moon **1** (1970) 190–231; © *D. Reidel Publishing Company, Dordrecht-Holland*

five orbiters, as shown in Table I. The amount of data is so great as to cause a handling problem even for modern high-speed computers. Its information content is correspondingly large. The data is described and discussed in terms of applicability to a gravity experiment in Section 3.

Modelling the motion of the orbiter presents no conceptual problems. Effects due to third bodies (i.e., Sun and Earth), radiation pressure, and low-order harmonics of the Moon's gravity field are readily accounted for. The practical problems associated with some of the effects, however, such as those due to the attitude control system on the one hand and the roughness of the Moon on the other hand, are a real challenge. Details of how these problems were handled in the mathematical model are discussed in Section 4.

2. Perspective and Results

Since the Moon is very nearly a uniform sphere, its gravity field is best described in terms of perturbations from the sphere. Three different representations are used here: spherical harmonic expansion, surface discrete mass distribution, and elevations referred to a uniform density spheroid. The last of these is used to construct gravity maps, as shown for example in Figure 1. The discrete mass distribution is effective in describing surface or near surface mass anomalies such as might be associated with visually observable features like the ringed maria. On the other hand, the global deviations from a sphere are more readily represented in spherical harmonics. During the early stages of the data analysis, emphasis was placed on the spherical harmonics. More recently, the discrete mass representation has yielded some interesting information. Thus we are simultaneously discovering facts about the small-scale surface gravity anomalies and the large-scale global fluctuations.

For proper perspective we review briefly the state of knowledge about the Moon's gravity field and mass distribution prior to the lunar orbiters. The only sources of factual information were the lunar libration data and the observed variations in the lunar ephemeris.

The Moon's mean radius is taken* as 1738 km. Its mass is 1/81.303 times that of the Earth, giving it a mean density (cf. [3]) of 3.34 g/cm^3, a little greater than that of common granite (2.78 g/cm^3). In comparison, the Earth has a mean density of 5.54 gm/cm^3. Thus, it would not be unreasonable to expect the moon to be of near uniform density throughout. One measure of the deviation from uniformity is the parameter $g=3C/2MR^2$ where C is the axial moment of inertia and R is the mean radius. For a uniform sphere, $g=0.6$. For a hollow uniform shell, $g=1.0$. Jeffreys ([4], p. 158) hypothesizes a value

$$g = 0.5956 \pm .0010. \tag{1}$$

Analysis of the physical librations leads to the following relations among the

* Sjogren, using Ranger impact data, suggests a value of the mean radius some 2.5 km smaller (cf. [5], p. 341).

TABLE I

Lunar Orbiter orbit data summary

Arc	Epoch t_0 Date	GMT	Duration T, days	Minimum height h, km[a]	Period, min	Semimajor axis a, km	Eccentricity e	Inclination i, deg[b]
IA	8/14/66	15:34	7.2	189	217	2765	0.3030	12.1
B1	8/21/66	09:51	3.8	56	209	2693	0.3337	11.9
B2	8/25/66	16:01	64.9	40	206	2669	0.3338	12.3
C	10/29/66	12:25	0.05 (crash)					
IIA	11/10/66	20:26	5.1	211	218	2760	0.3005	11.9
B	11/15/66	22:58	22.9	50	209	2690	0.3359	11.9
C	12/08/66	20:36	126.5	43	210	2702	0.3405	17.6
D	4/14/67	09:01	73.9	68	209	2692	0.3290	16.8
E	6/26/67	07:01	105.9	113	212	2715	0.3181	16.6
F	10/11/67	05:55	0.1 (crash)					
IIIA	2/ 8/67	21:54	5.8	110	215	2749	0.2903	21.0
B	2/12/67	18:13	59.0	54	208	2688	0.3335	20.9
C	4/12/67	17:40	95.3	59	208	2680	0.3295	21.5
D	7/17/67	01:21	44.8	143	212	2722	0.3088	21.0
E[c]	8/30/67	19:39	39.6	144	131	1968	0.0437	20.9
F	10/ 9/67	09:33	0.02 (crash)					
IVA	5/ 8/67	15:09	27.3	2706	721	6149	0.2769	85.4
B	6/ 5/67	23:16	3.0	75	501	4821	0.6239	85.1
C[d]	6/ 8/67	22:39	38.5	64	344	3752	0.5163	84.4
VA	8/ 5/67	16:49	1.6	198	505	4851	0.6015	85.0
B	8/ 7/67	08:44	1.8	100	501	4822	0.6187	84.6
C	8/ 9/67	05:08	62.6	100	191	2535	0.2763	84.6
D	10/10/67	19:37	112.4	200	225	2831	0.3155	85.1
E	1/31/68	06:13	0.073 (crash)					

[a] Minimum height above surface.
[b] Inclination to lunar equator.
[c] Apollo type, $e \approx 0$.
[d] Lost contact.

moments of inertia (cf. [3], p. 28):

$$\begin{aligned} \alpha &= (C-B)/A = 0.000397 \pm 0.000008\,, \\ \beta &= (C-A)/B = 0.000627 \pm 0.000001\,, \\ \gamma &= (B-A)/C = 0.000230 \pm 0.000006\,, \\ f &= \alpha/\beta \qquad\quad = 0.633 \pm 0.011\,, \end{aligned} \tag{2}$$

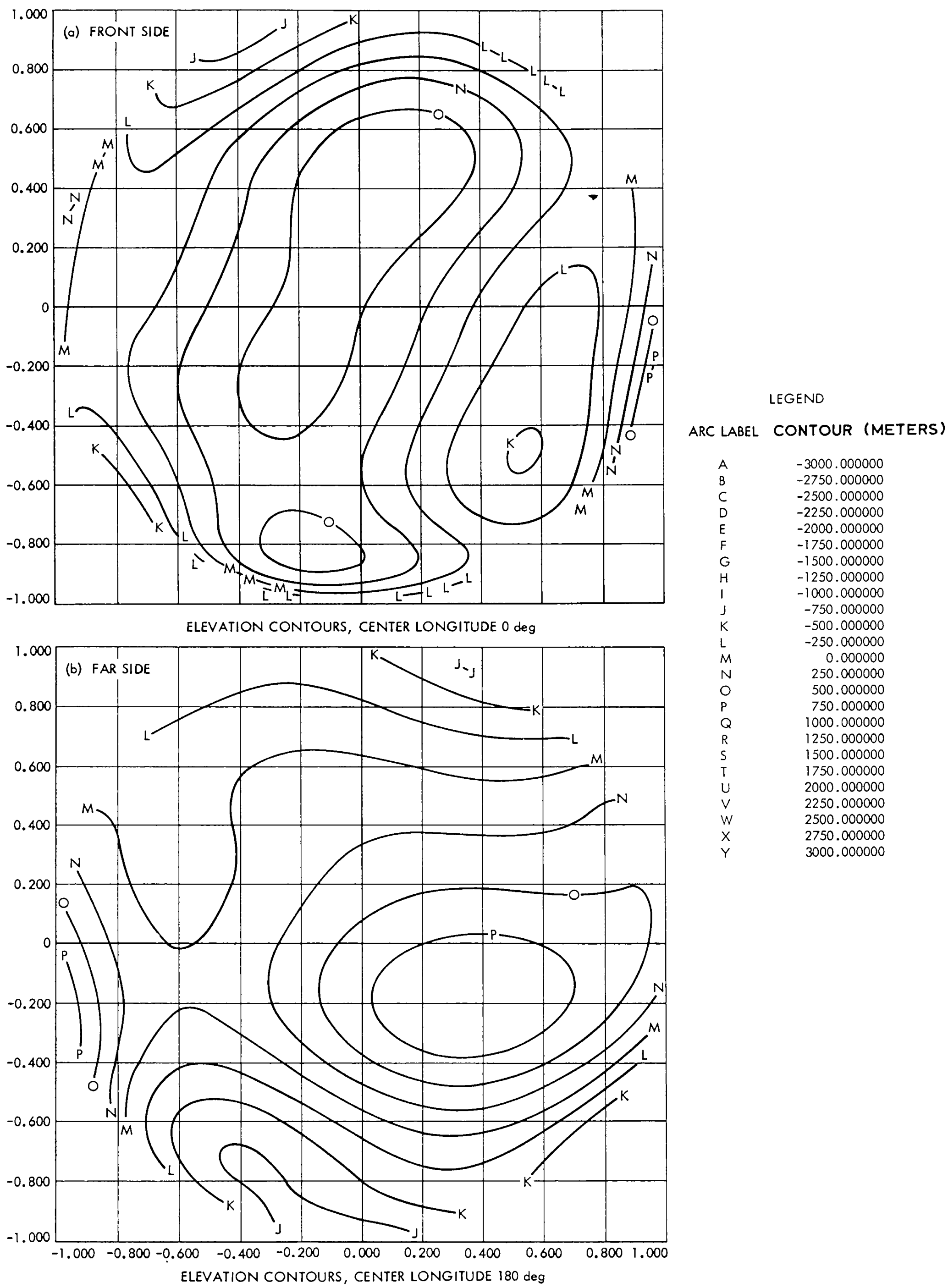

Fig. 1. Contour plot of mod-3.

in which A, B, C are the three principal moments of inertia listed in increasing size. To a first approximation, the value of β was obtained using Cassini's laws and the measured values of the Moon's axial and orbital inclinations. More detailed analysis was required for the determination of α and γ, which depend on very painstaking observations of the physical librations.

On the other hand, perturbational analysis of the lunar ephemeris, which has the potential for determining some of the inertia related constants, gives ambiguous results (cf. [6]). Specifically, if the unaccounted for nodal motion is attributed to mass distribution, and if the value of β is that given above, then the parameter g has the value 0.965, corresponding to a spherical shell rather than a nearly uniform density solid sphere. Eckert concludes that more study of the residuals in the node and perigee motion is required. In the meantime, the best estimate for g is that for near uniform density, as given by Equation (1) above.

An indirect estimate of the moment of inertia ratios can be obtained by assuming hydrostatic equilibrium. The value of β given above is some 17 times as large as the equilibrium value. Thus if any reliance is to be placed on the libration data, it must be concluded that the moon is far from hydrostatic equilibrium.

In summary, then, the pre-orbiter Moon was thought to be a triaxial spheroid, of near uniform density. The moment of inertia ratios α, β, γ were known to about two or three significant figures. There was no information on the fine structure of the gravity field.

Lunar Orbiter opened a whole new vista of information. The first data received were both illuminating and enigmatic. It contained an unmistakably strong signature of the Moon's gravity anomalies, and at the same time it presaged the difficulties inherent in extracting the information.

As subsequently revealed, the Moon is very rough. In mathematical language, the spherical harmonic coefficients up to a comparatively high degree are significant for the data. Consequently, a direct regression analysis, aimed at solving for the harmonic coefficients, is bound to have difficulty. There are three main sources of trouble: (1) the number of undetermined harmonic coefficients of importance is very large, (2) the coefficients are highly correlated with respect to the data, and (3) the amount of data required for the analysis is so large as to require excessive computer time. It was therefore found advantageous to go to a two-stage data analysis scheme, as described in Section 4.

An 8–4 gravity model was used as a reference standard for fitting the data, i.e., all harmonics up through degree 4 plus zonals up through degree 8 were included (see Section 4 for definition of the harmonic coefficients). In addition, solar radiation pressure was estimated for portions of the data.

Truncated models (with fewer harmonics) were also used, as explained below. Thus several sets of harmonics have been obtained, using basically the same data, i.e., all the extended mission data from all five orbiters.

Before describing the outcome of the regression analysis, we should note the connections between the moment of inertia ratios, α, β, γ of Equation (2), the parameters f and g and the second-degree harmonic coefficient C_{ij} and S_{ij}.

The second-degree harmonics are mathematically related to the moments of inertia as follows:

$$C_{20} = -\frac{C - \frac{1}{2}A - \frac{1}{2}B}{MR^2}, \tag{3}$$

$$C_{22} = \frac{B - A}{4MR^2}, \tag{4}$$

while C_{21}, S_{21}, and S_{22} are proportional to the second-degree products of inertia.* By simple manipulation, to first order of small quantities,

$$C_{22} = -\tfrac{1}{2}C_{20}\left(\frac{1 - f}{1 + f}\right), \tag{5}$$

$$g = -\frac{3C_{20}}{\beta(1 + f)}, \tag{6}$$

$$f = -1 + \frac{2C_{20}}{C_{20} - 2C_{22}}. \tag{7}$$

Thus, C_{20} describes the equatorial bulge of the Moon, often referred to as the oblateness. Its value is about -2.0×10^{-4}, or about one-fifth that for the Earth. The coefficient C_{22} measures the ellipticity of the equator, and has magnitude roughly ten percent that of C_{20}. Since A is the moment of inertia about the axis towards the Earth, and since the Moon has a bulge towards the Earth, C_{22} must be positive. These facts were known, and deducible from the numbers in Equations (1) and (2). We will show in the following the degree to which the lunar orbiter data corroborates and extends this information.

The end products of the two-stage regression analysis on the data are the seven sets of harmonic coefficients, JPL models 1 through 7 (mod-1–mod-7), listed in Tables II and III. Of these, mod-3 is in one sense the most complete since it is an 8–4 model and is based on all the data from the extended missions of all five orbiters. It was the outcome of three passes through the data. The LaRC Sept. 4 model** (Table II, column A) was used for the first pass through the data, and JPL mod-2 and mod-3 for the next two passes. However, since the computations were being performed at the same time that the data was being accumulated, each successive pass included more data, and it was only the last pass leading to JPL mod-3 that included all the data.

JPL mod-4 and mod-6 use all the data, but fit it to smaller sets of harmonics. In mod-4, the only non-zonals in the fit are C_{31} and S_{31}. The value of C_{22} was chosen *a priori* to be compatible with the libration data values of f and β. Mod-6 was similarly obtained, except for the inclusion of C_{41} and S_{41} also.

* See Equation (8).

** LaRC is continuing work on the problem and has published models based on more complete analysis of the data than the Sept. 9 model referred to here; see, for example, [26].

TABLE II

Harmonic models of lunar gravity

Parameter	Gravity models: $GM_{☾} = 4902.78$ in all models							
	LaRC, Sept. 4	JPL-1	JPL-2	JPL-3	JPL-4	JPL-5	JPL-6	JPL-7
$C_{20} \times 10^4$	−2.0480	−2.0263	−1.9189	−1.9564	−2.0086	−2.2021	−2.0010	−2.3387
$S_{21} \times 10^4$	−0.0651	0.0150	0.0221	0.1290				
$C_{21} \times 10^4$	−0.1398	−0.0878	0.0430	−0.1279				
$S_{22} \times 10^4$	−0.0375	0.1310	−0.0596	0.1014				
$C_{22} \times 10^4$	0.2445	0.2191	0.1123	0.1587	0.2258[a]	0.2258[a]	0.2258[a]	0.2258[a]
$C_{30} \times 10^4$	0.9049	−0.2223	−0.1483	−0.1299	−0.1321	−0.1744	−0.0994	−0.2923
$S_{31} \times 10^4$	0.1555	0.0740	0.1036	0.0948	0.0893	0.0646	0.0884	0.0940
$C_{31} \times 10^4$	0.2358	0.3636	0.3449	0.3493	0.3601	0.3031	0.3507	0.3364
$S_{32} \times 10^4$	0.1339	−0.0200	0.0277	0.0283				
$C_{32} \times 10^4$	−0.0384	−0.0257	0.0003	0.0076				
$S_{33} \times 10^4$	−0.0073	−0.0496	−0.0308	−0.0447				
$C_{33} \times 10^4$	0.0189	−0.0265	0.0353	0.0284				
$C_{40} \times 10^4$	0.2055	0.0941	0.1703	0.1230	0.1041	0.1054	0.0974	−0.3914
$S_{41} \times 10^4$	−0.0930	0.0564	0.0755	0.1099			0.0640	0.0423
$C_{41} \times 10^4$	−0.0714	−0.1237	−0.1063	−0.1607			−0.1163	−0.1141
$S_{42} \times 10^4$	0.0293	0.0051	0.0009	0.0012				
$C_{42} \times 10^4$	0.0223	0.0361	0.0353	0.0265				
$S_{43} \times 10^4$	0.0065	−0.0277	−0.0009	0.0148				
$C_{43} \times 10^4$	0.0107	0.0164	0.0232	0.0027				
$S_{44} \times 10^4$	−0.0034	0.0079	−0.0031	0.0001				
$C_{44} \times 10^4$	−0.0002	0.0091	−0.0058	0.0039				
$C_{50} \times 10^4$		−0.1614	−0.0123	−0.0365	−0.0721	0.0380	−0.0965	−0.0843
$C_{60} \times 10^4$		−0.1089	−0.0808	−0.0978	−0.0070	0.2647	−0.0475	−0.3219
$C_{70} \times 10^4$		0.1734	0.3178	0.2603	0.2396	0.3975	0.1870	0.3248
$C_{80} \times 10^4$		−0.2011	−0.1475	−0.0905	0.0622	0.0445	0.0231	−0.1166
F, km s^{-2}		1.211×10^{-10}	3.2897×10^{-10}	[b]	[b]	[b]	[b]	[b]

[a] Based on libration data and Koziel's results.

[b] Radiation pressure acceleration different for each arc as shown in Table X, last column.

TABLE III

Normalized[a] harmonic coefficients $\times 10^4$

Parameter	Gravity model					
	JPL-1	JPL-2	JPL-3	JPL-4	JPL-5	JPL-6
C_{20}	−0.9062	−0.8582	−0.8749	−0.8983	−0.9848	−0.8949
S_{21}	0.0116	0.0171	0.0999			
C_{21}	−0.0680	0.0333	−0.0990			
S_{22}	0.2030	−0.0923	0.1571			
C_{22}	0.3394	0.1739	0.2458	0.3498	0.3498	0.3498
C_{30}	−0.0840	−0.0560	−0.0491	−0.0499	−0.0659	−0.0376
S_{31}	0.0685	0.0959	0.0877	0.0827	0.0598	0.0818
C_{31}	0.3366	0.3193	0.3233	0.3334	0.2806	0.3247
S_{32}	−0.0585	0.0810	0.0829			
C_{32}	−0.0753	0.0008	0.0221			
S_{33}	−0.3558	−0.2209	−0.3205			
C_{33}	−0.1899	0.2533	0.2040			
C_{40}	0.0314	0.0568	0.0410	0.0347	0.0351	0.0325
S_{41}	0.0595	0.0796	0.1159			−0.1226
C_{41}	−0.1303	−0.1120	−0.1694			0.0675
S_{42}	0.0227	0.0042	0.0054			
C_{42}	0.1615	−0.1580	0.1185			
S_{43}	−0.4626	−0.0153	0.2480			
C_{43}	0.2736	0.3890	0.0458			
S_{44}	0.0332	−0.0132	0.0002			
C_{44}	0.0383	−0.0246	0.0163			
C_{50}	−0.0487	−0.0037	−0.0110	−0.0217	0.0115	−0.0291
C_{60}	−0.0302	−0.0224	−0.0271	−0.0019	0.0734	−0.0132
C_{70}	0.0448	0.0821	0.0672	0.0619	0.1026	0.0483
C_{80}	−0.0488	−0.0358	−0.0219	0.0151	0.0108	0.0056

[a] Normalization factor (See [25], p. 7):

$$(C_{nm})_{norm} = \left[\frac{(n+m)!}{(n-m)!\,(2n+1)\,(2-\delta_{0m})}\right]^{1/2} (C_{nm})_{not\,norm}.$$

Mod-5 (colum F) is the result of fitting eccentricity data only, but otherwise using the same procedure as for mod-4.

The last model of the JPL series (mod-7) is based on data from low inclination orbits only, i.e., from Lunar Orbiters I, II, and III, but no data from Orbiters IV and V.

Thus, seven different gravity models have been evolved, each purporting to represent the orbiter data, or portions thereof. We shall interpret these models at first in terms of the physical meaning of the parameters. Then, we will consider the associated statistics and the goodness of fit to the data.

To begin with, note the second-degree harmonics. As seen in Equations (1)–(7), of the five parameters C_{20}, C_{22}, β, f, and g, only three are independent. The first two are determined by the orbiter data, the next two by the libration data, and the last only by a combination. Thus, there is a one degree of freedom redundancy in the combined orbiter and libration data. Eventually, perhaps, it will be feasible to effect a simultaneous fit to all the data. However, at present because of the difficulties in the orbiter data mentioned above this has not been done. Instead, independent data fits have been obtained, and the resulting models compared with the help of Table IV.

The table has been constructed using a fixed value of β, namely the libration value. In the first four rows, the libration value of f and the orbiter data value of C_{20} are assumed known, and the values of g and C_{22} computed. Of the four models, mod-1 yields the value of g closest to Jeffreys'. The mod-3 and mod-6 values are smaller, but not unreasonable. The mod-7 value, since it implies a high density surface for the Moon seems improbable.

TABLE IV

Comparison[a] between libration and Lunar Orbiter results

Gravity model	Parameters			
	f	g	$-C_{20} \times 10^4$	$C_{22} \times 10^4$
JPL-1	0.633[b]	0.5937	2.0263[b]	0.2277
JPL-3	0.633[b]	0.5732	1.9564[b]	0.2198
JPL-6	0.633[b]	0.5863	2.0010[b]	0.2249
JPL-7	0.633[b]	0.6852	2.3387[b]	0.2628
JPL-1	0.644	0.5897	2.0263[b]	0.2191[b]
JPL-3	0.721	0.5439	1.9564[b]	0.1587[b]
JPL-3	0.572	0.5936[b]	1.9564[b]	0.2666
–	0.633[b]	0.5956[b]	2.0328	0.2284

[a] $\beta = (C - A)/B = 0.000627$.

[b] These values are fixed, and the remaining values are obtained using Equations (5) and (6) in the text.

In rows 5 and 6, the comparison is based on the orbiter values for C_{20} and C_{22}. Of interest here is the fact that the two values of f straddle the critical value $f = 0.662$.

Row 7 shows the values that f and C_{22} must have to be compatible with the mod-3 value of C_{20} and Jeffreys' g.

Row 8 gives the C_{20} and C_{22} values based entirely on libration data plus Jeffreys' g.

It is seen from Table IV that of all the JPL models, mod-1 gives best agreement with libration data, and Jeffreys' value of g. On the other hand, as we shall see later, mod-3 and mod-6 are best fits to all of the orbiter data, whereas mod-1 fits only part of it.

The remaining second-degree harmonics are related to the second-degree products of inertia as follows:

$$\left.\begin{aligned} C_{21} &= I_{zx}/MR^2, \\ S_{21} &= I_{yz}/MR^2, \\ S_{22} &= I_{xy}/2MR^2, \end{aligned}\right\} \quad (8)$$

in which the subscripts x, y, and z refer to the axes of the moments A, B, and C respectively.

When the coordinate axes are chosen to coincide with the principal axes of the Moon, the products of inertia and hence the coefficients C_{21}, S_{21}, and S_{22} all vanish. On the other hand, in practice the coordinate axes are chosen to correspond to the principal axes of an idealized Moon. Thus, precise measurements could conceivably yield non-zero values.

The magnitudes of the harmonic coefficients C_{21}, S_{21} and S_{22} are therefore a measure of the discrepancy between the two sets of axes. If the Euler angles between them designated by ϕ, θ, and ψ (cf. Figure 2) are assumed small, then it can be shown* that [7]

$$C_{21} = \theta\phi (C_{20} + 2C_{22}) + 4\theta\psi C_{22}, \tag{9}$$

$$S_{21} = - \theta (C_{20} + 2C_{22}), \tag{10}$$

$$S_{22} = 2(\phi + \psi) C_{22}. \tag{11}$$

Thus, C_{21} is of second order in the angles, while S_{21} and S_{22} are of first order. Their magnitudes for a rotation through 1° in each angle, and for nominal values of C_{20} and C_{22} are

$$\left.\begin{aligned} C_{21} &\sim - 0.11 \times 10^{-6}, \\ S_{21} &\sim 4 \times 10^{-6}, \\ S_{22} &\sim 1.6 \times 10^{-6}. \end{aligned}\right\} \tag{12}$$

However, it is difficult to reconcile the observations of the lunar librations with values of the Euler angles as large as 1°. For example, Jeffreys' analysis [8] yields an uncertainty in the inclination of the lunar equator of at most 30″ of arc, which should bound θ. Thus $|\theta| < 0.0015$, whence both C_{21} and S_{21} become negligibly small with

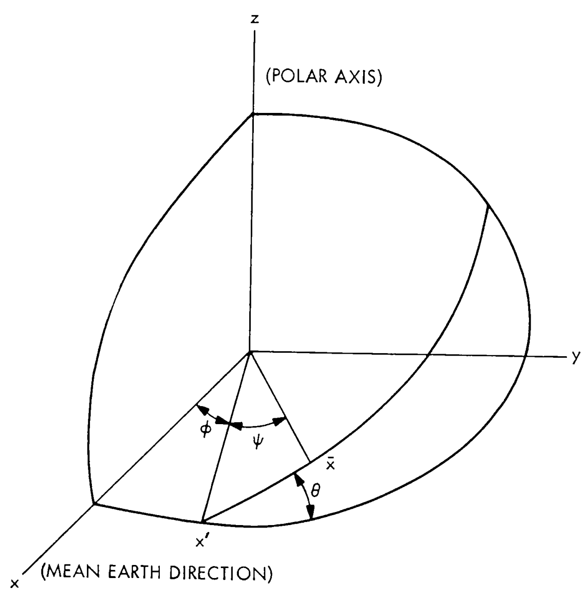

Fig. 2. Angles between principal axes and coordinate axes.

* The axes offset error induced in C_{20} and C_{22} is negligible for small angles.

respect to their effect on a lunar orbiter. However, S_{22} which does not contain the factor θ could possibly be significant if the principal axis in the earth direction were appreciably off the X-axis.

In view of these comments, then, the numbers in Table II can be interpreted as indicating an appreciable bias of the directions of the principal axes. For example, the mod-3 harmonics indicate angular values beyond the linear range assumed for Equations (9)–(11). For this reason, the data was reevaluated after mod-3 was obtained, using zero values for C_{21}, S_{21}, and S_{22} and an *a priori* value for C_{22}. Four new models were generated (cf. Table II, mod-4–mod-7), in which only the zonals and a few key tesserals were included. The value for C_{22} was taken to be compatible with the libration values for β and f, Equation (2), and the estimated value of C_{20} in mod-4.

In setting up these models, consideration was given to the fact that the two-stage data reduction procedure is intrinsically most effective in determining the zonal harmonics. The 31 and 41 coefficients were included because firstly they are next to the zonals in sensitivity for this procedure, and secondly, the more general analysis has shown them to be significantly large, especially C_{31}. This brings us to a discussion of the higher degree harmonics.

Mod-3 contains, besides the zonals to degree 8, all the second, third, and fourth degree tesserals. In order to compare the coefficients on the basis of size, it is proper first to normalize (cf. Table IV), for then the coefficients of equal size have comparable effect on the orbit. Accordingly, we find that in mod-3 the normalized coefficients C_{20}, C_{22}, C_{31}, S_{33}, C_{33} and S_{43} are the only ones larger in magnitude than 0.2×10^{-4}. The second-degree harmonics have already been discussed in terms of the lunar librations and the moments of inertia. Thus, C_{20} being associated with the axial moment of inertia is expected to be large for a rotating body. The coefficient C_{22} measures the bulge along the Earth–Moon axis, and it too can be expected to be large. The fact that the values of C_{20} and C_{22} differ widely from those to be expected for fluid equilibrium is another matter.

For the other large coefficients, the statistics of the analysis (cf. Table V) show that C_{31} is determined (percentagewise) an order of magnitude more accurately than C_{33}, S_{33} or S_{43}. Furthermore, as noted above, engineering considerations suggest that C_{31} is more sensitive to the data than these other coefficients. It follows therefore that if any credence is to be placed in the data, the value of C_{31} must be significantly large. Any gravity model must include C_{31} if it is to realistically represent the lunar gravity field.

Mod-4 and mod-6 represent truncated sets of harmonics, including all the zonals to degree eight but only some of the first order tesserals. It is noteworthy that the omission of the tesserals does not greatly affect the values of the remaining coefficients. Furthermore, the fit to the data, as will be seen later, is not greatly deteriorated.

Mod-5 was the result of an attempt to isolate the effect of eccentricity in the data. The results are not conclusive, especially in view of the fact that the data fit was much worse.

TABLE V

Standard deviations for JPL mod-3 harmonics, not normalized[a]

l	m	C_{lm} [b]	S_{lm} [b]
2	0	0.99	
2	1	3.91	3.14
2	2	2.84	2.70
3	0	1.72	
3	1	0.38	0.40
3	2	0.43	0.40
3	3	0.76	0.62
4	0	0.88	
4	1	1.17	1.03
4	2	0.47	0.59
4	3	0.47	0.42
4	4	0.12	0.11
5	0	1.67	
6	0	2.55	
7	0	2.11	
8	0	2.50	

[a] These standard deviations are based on an assumed weight of 0.1 Hz for the Doppler observations, with 60-s count time.
[b] Times 10^{10}.

In mod-7, the high inclination orbit data was omitted. The resulting high values of C_{20} and C_{40} are due to their correlation with respect to the low inclination data, while the value of C_{31} is not much affected. The expectation that this model might have application to Apollo navigation did not materialize.

Thus, we have exhibited gravity models expressed as spherical harmonics, based on the two-stage regression analysis of all the data. In contrast, we are presently developing discrete mass models based on short arc fits to the data. This work is currently in progress, and will be reported elsewhere. A preliminary report has already appeared in *Science* [9].

The gravity models, whether in terms of spherical harmonics or mascons can be represented graphically to show the equivalent distortions of a uniform density figure. Mod-3 is so represented in Figure 1. For contour maps of the other models, see [10]. It may be of some interest to try to associate the high points of these maps with the circular maria, as suggested by the mascon analysis. The correlation is not very good, but then the degree of the harmonic expansion is not large enough to be effective for this purpose.

3. The Data

A. DOPPLER RESIDUALS

The raw data for the selenodesy experiment consists of doppler and range obtained at S-band frequency by the NASA Deep Space Network (DSN). A description of the data and its processing is described (see [11]). The data itself, together with derived normal points and pertinent graphs and statistics has been collected under one cover in another JPL report (see [10]). Thus, the present discussion can be limited to a brief review of the data, and a commentary on its adequacy for a gravity experiment.

At the outset, it must be emphasized that the data itself is extremely precise. The noise level is orders of magnitude below the amplitude of the information signals. In one sense, therefore, this is a deterministic problem rather than a statistical one. However, in a larger sense, the gravity field itself must be looked at statistically, for the number of significant harmonic coefficients is very large, and have unknown amplitudes which can be assumed as randomly distributed. The effect of these coefficients on the raw data is a bias. Only when the normal points (compressed data) are evaluated does the statistical effect become evident.

For the data analysis, the fundamental unit of study is the Doppler residual curve (range is of secondary importance in the present context). Consisting of Doppler residuals plotted as a function of time, each curve contains the signature of the unmodelled parameters in the physical and engineering system surrounding the spacecraft.

Figure 3 shows a typical Doppler residual curve obtained from Lunar Orbiter 1. The ordinate is the frequency residual (observed-computed) in Hz.* Each point represents the frequency obtained by counting Doppler cycles over a fixed time interval,

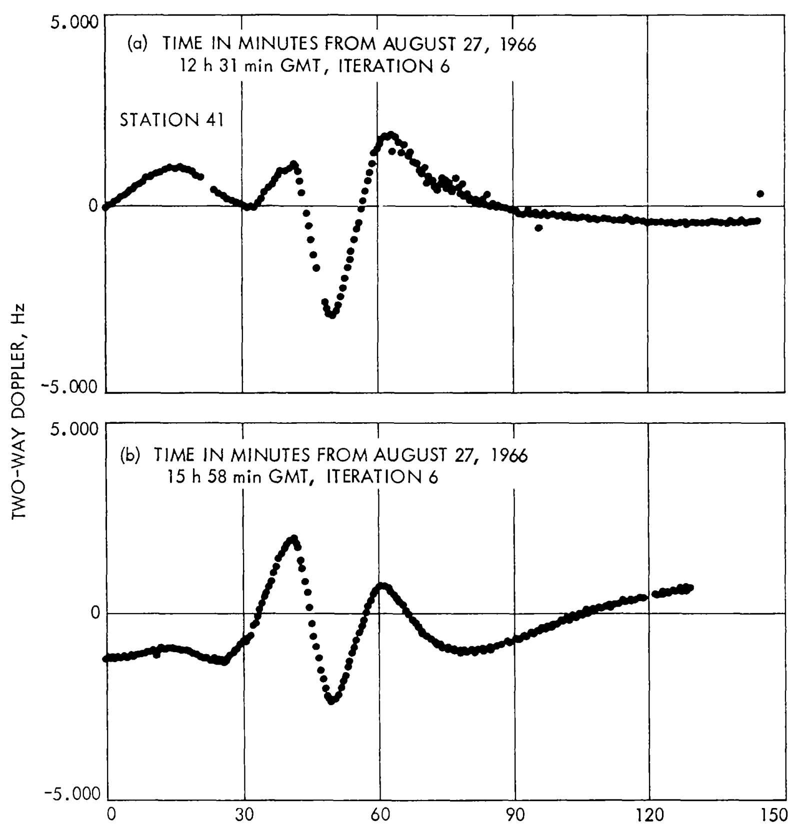

Fig. 3. Doppler residual curve, Lunar Orbiter I.

* At S-band (2300 MHz), 1 Hz = 65 mm/s.

in this case 30 s. To obtain this curve, the observed frequencies are fitted using a known gravity model (in this case the LaRC Sept. 4 model) and adjusting any of a set of parameters available in the computer program. In this case only the cartesian components of the spacecraft at epoch (i.e. the state at epoch) were adjusted.

Figure 3 includes two full orbits (less occultation time) of data from one station, typical of the data batches used for the normal points, although the inclusion of data from more than one station is preferable. The strength of the fit, and therefore the weight of the normal point is appreciably improved when 3-way data is available, i.e., data from two stations simultaneously, one transmitting and receiving, the other receiving only.

The noise level of the data is easily seen to be much below the signal level. Only in the short span after the 60-min mark of the first orbit is the noise visible, and here it is attributed to interference from photo readout.

Periselenium, or point of closest approach to the lunar surface occurs at 13 h, 14 min, 44 s, or at about 44 min along the abscissa of orbit 1 in the figure. Typically, the residuals exhibit a high amplitude oscillation near periselenium, as shown here. Unfortunately, these residuals cannot be interpreted directly as accelerations, except in certain special cases as will be mentioned below.

The nature of the orbit fitting process (least-squares differential correction) is such that orbit or model errors tend to produce maximum residuals near periselenium. The main reason for this is that the motion near periselenium is most sensitive to orbit disturbances even those not associated with lunar gravity. Another factor is the data spacing which for operational reasons is always uniform in time, thus tending to under-weight the data in the periselenium region. Still another factor is the fact that the Moon's gravity anomaly forces are stronger when the spacecraft is closest to the Moon.

As a result, the residual pattern and the problem of analyzing it has been nicknamed the periselenium wiggle problem.

Recently, Muller and Sjogren [9] have been ingenious enough to devise a scheme for extracting the spacecraft accelerations directly from the residual plots. Their procedure depends on two factors, choosing a data span of the proper length (usually about 40 min for a close orbit) and using a very simple Moon model, either spherical or triaxial. The short span has the effect of suppressing residuals due to large scale effects, since these can be absorbed in the state vector in a short arc. The simple Moon model avoids the introduction of extraneous residuals. By this procedure, it has been possible to develop a surface gravity map of the Moon, showing the stronger gravity anomalies and correlating them with surface features. The work is currently in progress, and will be reported separately.

It would be misleading to use only the one residual plot (Figure 3) to illustrate the data, which is in fact quite varied, depending on so many factors such as the orbit shape and geometry, the tracking pattern, the gravity model and the length of the data span. For example, data from a high orbit gives much smaller amplitude residuals as shown in Figure 4. At the scale plotted, the noise on the data is clearly identified.

In Figure 5, for a close-in near-circular orbit, the residuals are large. However, since periselenium is not sharply defined for a near circular orbit, the residuals remain large everywhere instead of clustering at periselenium.

As already noted, the internal consistency of the Doppler data is excellent, giving an accuracy of the order of 0.02 Hz (cf. Figure 4). However, due to model uncertainties, primarily of the lunar gravity field, the position and velocity of the spacecraft cannot be determined with equivalent precision. Typically, there is an uncertainty of the order of kilometers in position, and m/s in velocity.

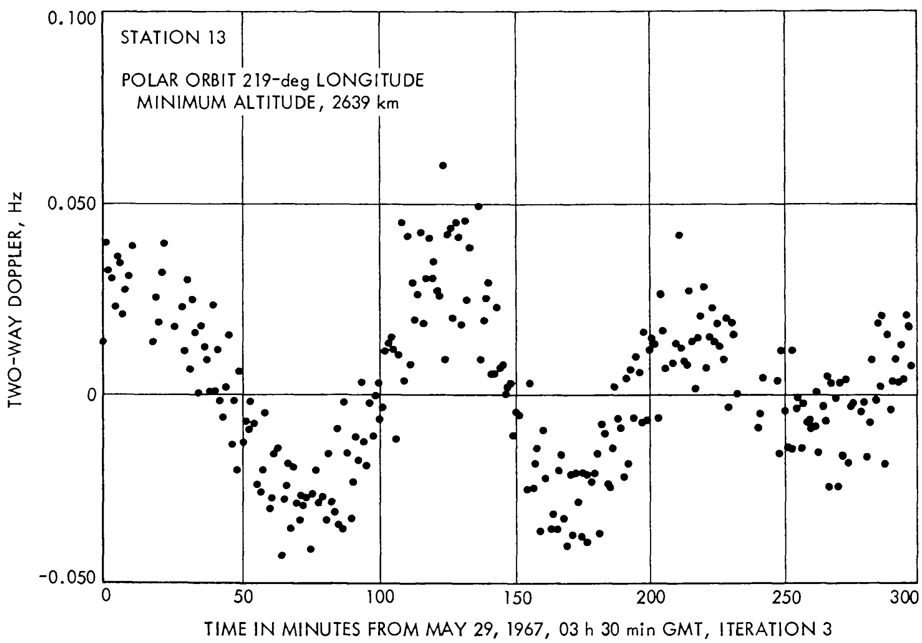

Fig. 4. Doppler residual curve, Lunar Orbiter IV.

In order to isolate the sources of error, an exhaustive list of possibilities was assembled, and investigated one by one. This study is reported in [12] in which it is shown that none of the error sources, excepting the unmodelled part of the lunar gravity field, can give rise to the observed residuals. By elimination, therefore, it is concluded that the lunar gravity field is the only possibility. The problem that remains, therefore, is how best to fit the data with a set of parameters consisting of gravity field coefficients and orbit parameters.

B. ORBIT FITTING DIRECTLY TO THE TRACKING DATA

The first practical problem to be solved for selenodesy was found very quickly to be that of fitting an orbit to a fairly short arc of data. Computer capacity limitations make fits to arcs in excess of 10 or 15 orbits impracticable. Furthermore, the longer the arc, the more detailed must be the gravity model. Thus it was decided that for the normal point analysis, the data compression unit should be approximately two orbits of data.

This choice was supported by several other considerations also: a shorter arc, of one orbit or less, gives a very weak orbit determination unless there is some three-way (i.e., two-station simultaneous) data; the tracking patterns are such as to allow two-orbit groupings in most cases, and still yield enough normal points to determine a trend; a two-orbit fit is usually effected with a reasonable number (e.g., four or fewer) iterations through the computer. Thus, mainly from practical considerations, the bulk of the orbit fitting was applied to data batches obtained from approximately two consecutive orbits.

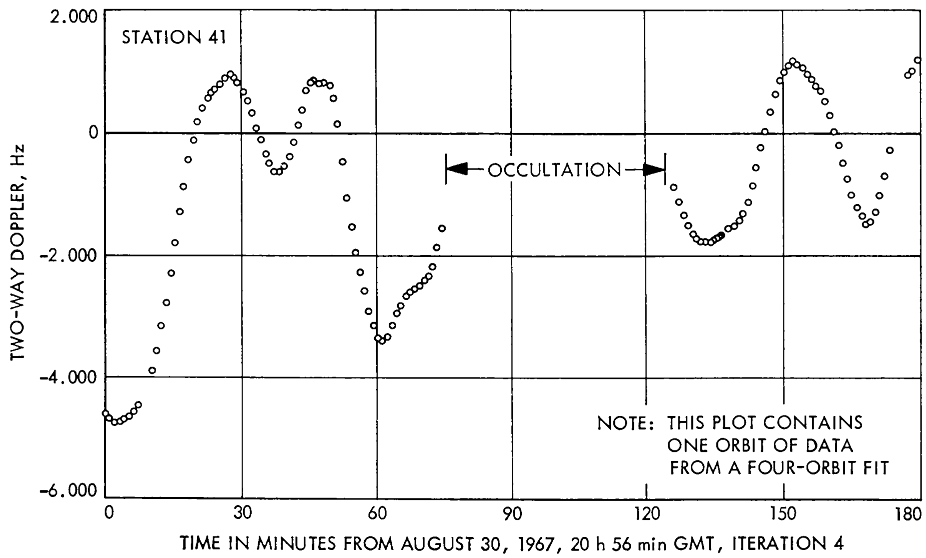

Fig. 5. Doppler residual curve, Lunar Orbiter III.

The principal tool for the fitting process (orbit determination or simply OD) was a computer program (SPODP = Single Precision Orbit Determination Program) based on differential correction and least squares, and operating in Moon-centered cartesian coordinates. For a detailed description of SPODP, see [13].

Due to the nature of the data, and the deficiency of the gravity model, the OD results do not reflect the precision of the Doppler observations. In the first place, the geometrical configuration very closely resembles that of a spectroscopic binary star, as described in [14], pp. 357–360. Thus, not all of the orbit parameters can be expected to be determinable, or if so only weakly at best. In particular, the node in the plane-of-the-sky is indeterminate for the spectroscopic binary, and hence almost indeterminate in the lunar orbiter case. Furthermore, the semimajor axis a (see Nomenclature) is determined in the combination $na \sin i$, and can be decoupled, only if the Moon's mass constant μ is separately identified. For a detailed discussion of determinacy in orbiters of remote primaries, see [15].

The problem, of course, with the spectroscopic binary is the lack of parallax in the OD geometry. For the lunar orbiter, parallax is introduced in three ways, the relative motion of Earth and Moon, the rotation of the Earth, and the use of two or more widely separated tracking stations. In the course of two orbits of tracking (6 h) the net parallax of some 4° more or less is adequate for the OD, but gives a weak determination of the orbit. The reason for the weakness, of course, is the interaction of the geometry with the incomplete gravity model, not any deficiency in the Doppler measurements.

One basis for measuring the adequacy of an OD is the statistics as given by the standard deviations and correlation matrix. For a typical one station two-orbit OD (residuals shown in Figure 3, statistics in Table VI) the standard deviations of the state, in cartesian coordinates show position good to 200 m, velocity to 100 mm/s. However, the correlation matrix belies this accuracy because of the extremely high correlations among all the parameters. Obviously, the node in the plane-of-the-sky is being very poorly determined.

In spite of the high correlations, the OD process converges, and the orbit so obtained proves adequate for mission orbit prediction. On the basis of separate studies, including comparisons between different Moon models, comparisons using simulated data, and comparisons based on the photographs of the lunar surface taken from the spacecraft, it has been found that the actual quality of the OD is an order of magnitude poorer than that given by the standard deviation of Table VI. Thus, an accuracy figure of 2 km in position and 1 m/s in velocity appears more realistic.

Without detailing the background studies, we now outline some of the assumptions and procedures used in the OD computations for the normal points. Underlying the whole procedure was a desire for consistency, resulting for example, in the use of a single gravity model for each pass through the data. An alternative procedure, which would produce smaller residuals, would be to tailor the gravity model to the orbit. At any rate, we list the following items as standard usage in the normal point OD:

(1) The mass constant of the Moon was fixed *a priori* at the Mariner II value $\mu = 4902.78$ (cf. [16]). More recent determinations using Mariner IV have confirmed this value ([17] gives $\mu = 4902.76 \pm 0.10$) while the Ranger values [17] are somewhat lower. Determinations of μ using Lunar Orbiter are weak because of correlation with the spacecraft orbit semimajor axis.

(2) Three-way data was used whenever available. The resulting strength in the OD overshadows the uncertainty in frequency bias.

(3) Although the OD has the capability of solving for frequency bias when simultaneous data from two or more stations is used, the bias was not solved for. It was found that the bias effect is small compared with the gravity model error effect, and that it is correlated so highly with the state vector with respect to the orbiter data as to make the solution meaningless.

(4) Ranging data, when available and compatible with the Doppler was used in the OD. Actually, the effect of the ranging data is small except when solving for a directly related quantity such as Earth–Moon distance.

(5) Gravity harmonics were not solved for.

(6) The Doppler data was given a weight of 0.1 Hz, the ranging data 15 m. These

TABLE VI

Statistics of two-orbit OD

Standard deviations			
km	X	.87438731	−01
	Y	.13218465	00
	Z	.15609255	00
km/s	DX	.11606215	−04
	DY	.44451985	−04
	DZ	.95042856	−04

Correlation matrix of estimated parameters

	X	Y	Z	DX	DY	DZ
X	.10000000 01	.99991336 00	−.99957268 00	−.99727233 00	.99953090 00	−.99943516 00
Y	.99991336 00	.10000000 01	−.99964653 00	−.59711537 00	.99961001 00	−.99936714 00
Z	−.99957268 00	−.99964653 00	.10000000 01	.99552304 00	−.99927252 00	.99914857 00
DX	−.99727233 00	−.99711537 00	.99552304 00	.10000000 01	−.99535362 00	.99479014 00
DY	.99953090 00	.99961001 00	−.99927252 00	−.99535362 00	.10000000 01	−.99991124 00
DZ	−.99943516 00	−.99936714 00	.99914857 00	.99479014 00	−.99991124 00	.99999999 00

numbers are reflected in the statistics of the estimated parameters (cf. e.g., Table VI) and therefore also in the weights associated with the nominal points.

(7) The epoch for each OD was chosen to avoid the periselenium region, and to be as close to the data as possible. Otherwise, the quality of the OD suffered.

Finally, before describing the normal points, we make some general comments as to the adequacy of the data for selenodesy. Since the primary aim of the selenodesy experiment is to determine the entire gravity field of the moon, the most effective set of observations are those that sample the greatest volume of near-lunar space. Furthermore, the dynamical sampling obtained by the orbiter tracking data has intrinsic peculiarities, because of the selective sensitivity of orbit. Thus, an adequate dynamical sampling should include several orbits, covering a range of inclination and semimajor axes. On this score, the Lunar Orbiter series is only marginally adequate.

As shown in the last column of Table 1, the range of inclination of the Lunar Orbiter was limited to two regions, low inclinations between 10 and 20° and high inclination, about 85°. The gap between 20 and 85° is a weakness in the coverage that is difficult to accommodate. The semimajor axis values, on the other hand, do provide good coverage in the radial dimension, although a few more orbits at intermediate and high altitude would be desirable to strengthen the low-degree harmonic determinations.

A characteristic of the orbits not given in Table I is the fact that periselenium position always occurs in the equatorial belt. For the low inclination orbits, of course, this fact is unavoidable. The high inclination orbits were purposely so designed because of the photography requirements. The net result is that the close-lunar region is sampled only at low latitudes, and biases the results accordingly.

Because the Moon rotates beneath the orbit once every 28 days the entire low latitude belt is sampled by a spacecraft tracked that long. Unfortunately, the Earth rotates around the orbit with the same 28 day period. The result is an occultation of the spacecraft, and a gap in the tracking data over the Moon's far side. It follows that any gravity model derived from the data must be biased in favor of near-side effects.

Operation and handling of the spacecraft itself had its damaging effects on the overall data usefulness. Of particular significance is the fact that the attitude control system was not coupled, either in pitch or in yaw (roll jets were coupled). Any torque about either the pitch or the yaw axis resulted in a control system reaction which produced a linear acceleration in addition to the torque compensation.

In the case of Lunar Orbiter, the spacecraft torques were produced by: (1) solar radiation pressure, (2) reflected (lunar) radiation pressure, (3) gravity gradient, (4) high-rate attitude maneuvers used for spacecraft operation, such as picture taking, and (5) low-rate attitude maneuvers used for spacecraft housekeeping chores, such as thermal control.

In theory, each of these torques can be modelled and the effect of the attitude control jet response on the trajectory accounted for. However, in practice this becomes very difficult, and to do it properly would be very expensive in man-hours, in computer programming, and computer running time. Furthermore, because of engineering uncertainties and incompleteness of the telemetry records, the reliability of the results would be in doubt. Finally, because these torques are generally not secular or periodic (e.g., the high-rate attitude maneuvers) they could not easily be incorporated in the averaged equations of motion.

Solar radiation pressure torque is close to being periodic, with the period of the orbiter. It is complicated by passage through the Moon's shadow. In any case, its effect is reasonably easy to model, and this has been done. The component of solar radiation pressure (including shadowing) and the associated attitude jet reaction in the direction of the sun-spacecraft line is accounted for in all our estimates. In fact, we sometimes solve for it.

Reflected (lunar) radiation pressure too is periodic, but is small enough to be neglected. Firstly, because of the low albedo of the Moon, the strength of the reflected radiation is less than 10% of that of the Sun. Secondly, the major spacecraft surfaces (the solar panels) are predominantly edge-on to the reflected radiation, thus reducing its effect.

Torque produced by gravity gradient is of the same order of magnitude as that produced by solar radiation pressure. It is strongest at closest approach to the Moon, and is periodic with half the period of the orbiter (it goes through four zeros each orbit). Figure 3 of [12] shows an example of the spacecraft attitude reaction to radiation pressure torque. In this example, the pitch direction was most affected. The increase in frequency of the pitch jet pulses near periselenium is dramatic. Since these pulses are at the low thrust level their net effect over one orbit is not appreciable, and so is not modelled. Over many orbits it can be appreciable, but the difficulty of modelling in the averaged equation makes it impracticable.

The commanded attitude maneuvers (high-rate maneuvers) are the most serious offenders in disturbing the orbit. During the photo phase of the Lunar Orbiter mission these maneuvers disturbed the orbit so much as to make the corresponding arcs unusable for selenodesy. During the extended mission, the number of such maneuvers was minimized. However, the low-rate maneuvers continued, producing an anomalous perturbation in the orbit elements.

Finally, but not last in importance for the adequacy of the data, the tracking patterns play a strong role. In general, and in deference to the operational problems in tracking many spacecraft with limited facilities and only one available frequency, the coverage was good. There were long arcs with almost daily tracking, such as IA and IIIB (see Table I). A large fraction of the normal point data batches included two stations and three-way data. On balance there can be no complaint on the basis of lack of coverage by the NASA DSN.

C. NORMAL POINTS

As noted in the previous paragraph, the data has been processed in batches, each of two or so orbits in length, and each batch represented by a normal point. Thus, the original data consisting of several thousand points were compressed into some 288 points distributed among the Orbiter arcs (see Table I) as follows:

Number of normal points in each arc	
IA–20	IIIC– 7
IB–55	IIID– 4
IIC–40	IIIE–18
IID–10	IVC–10
IIE– 4	VC–34
IIIB–56	VD–30

The unevenness of the distribution results from the unevenness in the tracking pattern. Some arcs such as IB, IIC and IIIB contain much more data than the others. Table 4 of [10] lists the epochs and initial state in cartesian coordinates for all of the data batches used to generate normal points. The raw data itself is available on magnetic tape from the NASA data library at Goddard Space Flight Center, Greenbelt, Maryland.

A normal point consists of the five Keplerian elements of the spacecraft orbit, a, e, i, Ω and ω referred to the ecliptic and equinox of 1950 together with a weighting matrix, W. The statistics associated with the normal point are given by the covariance matrix, which is the inverse of W. Tables 2 and 3 of [10] list the normal points, the weighting matrices, the covariance matrices, and correlation matrices for all 288 normal points obtained for the last iteration through the data, and based on the JPL model-2 representation of the Moon's gravity. An example is shown in Table VII of this report.

The first row of Table VII gives the Keplerian elements derived for the normal point, and corresponding to the time average over one orbit centered in the data span. The W-matrix listed next is the information matrix used to weight the normal point. Next is the W-inverse or the covariance matrix whose diagonal terms are in a general way linked to the standard deviations. The square roots of these diagonal terms are shown on the last line. If interpreted as standard deviations (which they should not be) they would indicate that for this batch of data the semimajor axis is determined to 0.2 meters, the eccentricity to 4×10^{-7}, and the angles to a few hundredths of a degree.

The correlation matrix is more directly meaningful. It shows that the orbit orientation is very poorly determined, particularly due to the high correlation between Ω and ω. As we shall see later, the sum $\Omega + \omega$ is a much better determined angle for the low inclination orbits, as might be expected.

A given batch of data are compressed into normal points in the following manner. Firstly, using the appropriate gravity model, the state of the spacecraft flight path at epoch (i.e., its cartesian coordinates) is determined. Secondly, using one orbit centered at the mid-time of the data span, the averaged values of the Kepler elements, together with their statistics (i.e., W-matrix) are computed. Details of the computation of W are given in the appendix of [10].

TABLE VII

Normal point and related statistic example taken from Lunar Orbiter arc IB

SMA = a(km) .26697435 04	ECC = e .33327958 00	INC = i(deg) .13363812 02	NODE = Ω(deg) .25871871 03	OMEGA = ω(deg) .18971692 03
W Matrix				
.28582456E + 08	−.21654879E + 10	.22150171E + 06	−.13318787E + 08	−.12139564E + 08
−.21654867E + 10	.68711929E + 13	−.19231193E + 10	.62767942E + 10	.50202531E + 10
.22150715E + 06	−.19231200E + 10	.65109644E + 08	.26298383E + 09	.27230264E + 09
−.13318778E + 08	.62767901E + 10	.26298384E + 09	.14525728E + 10	.14625924E + 10
−.12139585E + 08	.50202595E + 10	.27230271E + 09	.14625924E + 10	.14759034E + 10
W Inverse matrix				
.46857612E − 07	.16246707E − 10	.86768554E − 06	.18900792E − 05	−.20327896E − 05
.16239849E − 10	.16529412E − 12	.58127616E − 09	.11966528E − 08	−.12935337E − 08
.86747827E − 06	.58170351E − 09	.71222565E − 04	.15424230E − 03	−.16598652E − 03
.18896455E − 05	.11975891E − 08	.15424357E − 03	.33438106E − 03	−.35981160E − 03
−.20323216E − 05	−.12945404E − 08	−.16598778E − 03	−.35981137E − 03	.38717918E − 03
Correlation Matrix				
.10000000E + 01	.18460632E + 00	.47496705E + 00	.47749530E + 00	−.47725047E + 00
.18452840E + 00	.10000000E + 01	.16941233E + 00	.16096025E + 00	−.16169368E + 00
.47485359E + 00	.16953688E + 00	.10000000E + 01	.99947946E + 00	−.99955811E + 00
.47738573E + 00	.16108619E + 00	.99948769E + 00	.10000000E + 01	−.99999619E + 00
−.47714059E + 00	−.16181952E + 00	−.99956569E + 00	−.99999555E + 00	.10000000E + 01
Square root of diagonal terms of *W* inverse				
.21646619E − 03	.40656379E − 06	.84393462E − 02	.18286089E − 01	.19676869E − 01

The normal points are the observed points for use in the second stage of the regression analysis. They are computed to be compatible with the Kryloff-Bogoliuboff averaged variables when this method is applied to the equations of motion of the spacecraft in Lagrange form. This interpretation and some of the mathematical background will be discussed in more detail in Section 4.

Though the covariance matrices for the normal points give standard deviations which measure the quality of the data, these standard deviations cannot usefully be interpreted as measures of the error in the usual sense. The difficulty arises because of the unmodelled biases in the computations. A much better error measure is found empirically by computing the same normal point several times using a different basis each time.

No attempt has been made to derive meaningful statistics on this basis. Rather, a sample pass of data has been fit to an orbit in each of several modes with the aim of finding the resulting dispersion in the averaged Keplerian elements. Table VIII lists the normal points calculated for a pass of Lunar Orbiter V data calculated in 10 different modes.

For the nominal case, there are some $2\frac{1}{2}$ orbits (8 h) of data, including 3 h of three-way. Thus, the data is strong for orbit determination. The alternate modes of computation include truncating or extending the data, eliminating three-way, and shifting the epoch.

A large change in the results is seen to be caused by truncating the data to 3 h, 45 min. However, the remaining cases seem to be more or less randomly scattered. The last column, showing the center time for the data used, is included to allow correction for secular trends in the elements. These secular rates (listed in the bottom row) are not large enough to reduce the dispersion appreciably.

Row 11 contains the total spread in the data, which is to be compared with the standard deviations (row 12) obtained from the computed statistics. The observed spread in the estimates is thus seen to be two orders of magnitude greater than the computed standard deviations.

Another basis for judging the quality of the normal points is the fit to the computed orbits. The most complete fit to the data is represented by JPL mod-3, an 8–4 model using all 12 data arcs. Plots of the residuals can be found in [10] (Fig. 4). Relevant statistics of the residuals are given here in Table IX. Listed first are the averages of the residuals, which are a measure of the trend in the data (with respect to the model). The standard deviations listed second measure the scatter.

The comparison of these standard deviations with the spread of the computed normal points in Table VIII is of particular interest. For semimajor axis, the values in Table IX run as high as 100 m for some arcs, as against 55 m in Table VIII, which for this type of computation is reasonably consistent. On the other hand, the Table IX values for the remaining parameters are about an order of magnitude greater than the corresponding ones in Table VIII.

Some of the arcs are much more poorly fit than others, even after overlooking those with only a few points. In particular, arc IIIE shows large dispersions. One expla-

TABLE VIII

Dispersion in normal point estimate, point VC-34

Row	Epoch, 8/22/67		Data span		Notes	Parameters[a]					T[b] 8/22/67	
	H	Min	H	Min		a, km 2535 +	$e \times 10^3$ 274 +	i, deg 83 +	Ω, deg 68 +	ω, deg 0 +	H	Min
1	4	15	7	47	Nominal	0.212	0.808	0.730	0.796	0.748	8	21
2	4	15	3	45	Short	0.157	0.763	0.574	0.892	0.253	6	03
3	4	15	5	45	Short	0.190	0.816	0.662	0.833	0.572	6	48
4	4	15	6	45	Short	0.195	0.806	0.676	0.828	0.585	7	33
5	4	15	13	45	Long	0.187	0.862	0.700	0.831	0.470	11	03
6	4	15	7	47	No 3-way	0.205	0.813	0.751	0.783	0.822	8	21
7	4	49	6	58	t_0[c] + 34 min	0.185	0.834	0.715	0.805	0.677	8	20
8	5	09	6	58	t_0 + 54 min	0.180	0.875	0.740	0.791	0.759	8	40
9	5	29	6	58	t_0 + 74 min	0.187	0.867	0.747	0.788	0.765	9	00
10	5	49	6	58	t_0 + 94 min	0.190	0.856	0.737	0.796	0.707	9	20
11	Spread of parameters:					0.055	0.100	0.177	0.096	0.569		
12	Standard deviations (based on OD):					0.0007	0.00085	0.0015	0.00029	0.0022		
13	Secular rates:						$\dot{e} = -0.00025$ per day	$di/dt = -0.191$ deg/day	$\dot{\Omega} = -0.072$ deg/day	$\dot{\omega} = 0.174$ deg/day		
	Epoch of pericenter passage = 5 h 09 min											
	Period = 3 h 11 min											

[a] a, e, i, Ω, ω are averaged Kepler elements, referred to ecliptic and equinox of 1950.
[b] T is the center time of the orbit used to determine the averaged elements.
[c] $t_0 = 4$ h 15 min is the epoch of the nominal orbit fit (row 1).

TABLE IX

Residuals for JPL mod-3

Arc	No. of points	Average residuals						Time span			Inc (deg)
		$a(m)$	$e(\times 10^6)$	i (deg)	Ω (deg)	ω (deg)	$\Omega+\omega$ (deg)	Day	H	Min	
IA	20	0.26	−46	−0.027	−0.061	0.057	−0.004	6	11	37	12
IB	55	−2.02	−175	−0.033	−0.501	0.445	−0.056	57	5	58	12
IIC	40	17.85	−1264	0.044	0.538	−0.700	−0.162	126	1	18	18
IID	11	−25.85	231	0.005	−0.756	0.622	−0.134	73	16	10	17
IIE	4	1.78	244	−0.003	1.587	−1.889	−0.302	94	9	22	16
IIIB	56	−79.55	140	−0.195	−0.389	0.394	+0.005	50	18	32	21
IIIC	7	3.74	−909	0.141	1.616	−1.298	+0.318	94	22	25	21
IIID	4	−0.75	1023	−0.076	−0.349	0.100	−0.249	44	8	40	21
IIIE	18	41.94	−2514	−0.024	2.074	−2.158	−0.084	39	7	1	21
IVC	10	−24.61	66	0.058	0.020	0.079	–	31	22	29	85
VC	34	−26.71	910	0.148	−0.155	0.092	–	53	3	17	85
VD	30	−64.09	−1102	0.445	0.308	−0.431	–	111	20	20	85
	288										

Standard deviations

Arc	$a(m)$	$e(\times 10^6)$	i (deg)	Ω (deg)	ω (deg)
IA	5.41	64	0.026	0.205	0.190
IB	63.97	358	0.268	0.751	0.790
IIC	56.90	1292	0.231	0.822	0.802
IID	58.03	586	0.412	1.054	1.076
IIE	9.93	218	0.044	2.239	2.600
IIIB	103.71	408	0.392	0.984	1.009
IIIC	42.75	1240	0.153	1.628	2.069
IIID	6.13	692	0.073	0.498	0.439
IIIE	57.99	2061	0.217	1.053	1.191
IVC	97.43	235	0.316	0.079	0.166
VC	95.39	655	0.568	0.174	0.704
VD	101.95	1147	0.497	0.318	0.512

nation is that since IIIE is a low almost circular orbit, the high-degree harmonics are relatively more important. Hence, the incompleteness of the model is more damaging.

The three different measures of dispersion discussed above each describe different aspects of the data reduction process, and therefore must all be retained for an adequate description of the data.

4. The Mathematical Model

A. BASIS FOR MODEL

In designing the computer software for the selenodesy data reduction, it was intended to include in the mathematical model all of the effects large enough to be statistically significant with respect to the quality of the data. Thus, the model includes the gravity field of the moon, expressed as a spherical harmonic expansion, the gravity effects of Earth and Sun and solar radiation pressure. Gravitational effects of the planets are too small to be worth considering. Dynamical implications of relativity, though practically negligible, have been included in the equations.

Modelling of the data itself was not considered part of the selenodesy problem, as this job had already been taken care of to more than sufficient precision for translunar and interplanetary spacecraft tracking. Thus, the basic computer program SPODP, was already available.

In general, the model is more than adequate for the selenodesy work, with two possible exceptions: the moon's gravity field, and the attitude control system effects. The gravity field model is limited to fourth-degree tesseral harmonics and eighth-degree zonals. It is intended that the whole gravity field be interpreted with respect to this truncated model, and that higher degree harmonic effects be absorbed as much as possible in it. The ultimate success of this approach will depend to a great extent on the roughness of the Moon, i.e., the size of the unmodelled high degree, harmonic coefficients. The attitude control system effects were not modelled directly, but rather incorporated in the solar radiation pressure coefficient. The ultimate effectiveness will have to be tested empirically by analyzing the residuals to the data fits.

B. METHOD OF AVERAGES

No computer system presently available can process economically the amount of data available from the Lunar Orbiter tracking without resorting to some type of data compression, and some means for rapid computation of trajectories. The difficulty stems from the fact that trajectories with a large number of orbits, perhaps several hundred, must be dealt with.

For the selenodesy orbits, the computer program was designed around trajectories computed by the method of averages. Effectively, only the orbit-to-orbit changes in the trajectory are considered, the in-period effects being entirely neglected.

The Keplerian elements a, e, i, Ω, ω and χ were chosen to represent the motion of the spacecraft, leading to the Lagrangian equations* (cf. [18], p. 289)

$$\begin{aligned}
\frac{\mathrm{d}a}{\mathrm{d}t} &= \frac{2}{na}\frac{\partial U}{\partial \chi},\\
\frac{\mathrm{d}e}{\mathrm{d}t} &= \frac{1-e^2}{na^2 e}\frac{\partial U}{\partial \chi} - \frac{(1-e^2)^{1/2}}{na^2 e}\frac{\partial U}{\partial \omega},\\
\frac{\mathrm{d}i}{\mathrm{d}t} &= \frac{\cot i}{na^2(1-e^2)^{1/2}}\frac{\partial U}{\partial \omega} - \frac{1}{na^2(1-e^2)^{1/2}\sin i}\frac{\partial U}{\partial \Omega},\\
\frac{\mathrm{d}\chi}{\mathrm{d}t} &= -\frac{2}{na}\frac{\partial U}{\partial a} - \frac{1-e^2}{na^2 e}\frac{\partial U}{\partial e},\\
\frac{\mathrm{d}\omega}{\mathrm{d}t} &= \frac{(1-e^2)^{1/2}}{na^2 e}\frac{\partial U}{\partial e} - \frac{\cot i}{na^2(1-e^2)^{1/2}}\frac{\partial U}{\partial i},\\
\frac{\mathrm{d}\Omega}{\mathrm{d}t} &= \frac{1}{na^2(1-e^2)^{1/2}\sin i}\frac{\partial U}{\partial i}.
\end{aligned} \tag{13}$$

in which U, the disturbing potential, includes the gravity effects of earth, sun, and the non-spherical part of the moon. Radiation pressure enters directly through the disturbing force representation rather than the potential.

The method of averages as developed in [19], Chapter 5, is applied to obtain a set of equations in the averaged variables, a, e, i, Ω, ω, and χ. Only the first approximation is used. Higher order approximations lead to much more complicated equations, and, as shown in [20], are not necessary for this application.

For details of the computation procedure used to integrate the equations, and fit the data, the reader is referred to the notation in [21].

C. MOON'S GRAVITY REPRESENTATION

Since the Moon is nearly a sphere, its gravity potential Φ should be representable as an expansion in spherical harmonics

$$\Phi = -\frac{\mu_{☾}}{r}\left\{1 + \sum_{n=1}^{\infty}\sum_{m=0}^{n}\left(\frac{R}{r}\right)^n P_n^m(\sin\phi)\,(C_{nm}\cos m\lambda + S_{nm}\sin m\lambda)\right\}. \tag{14}$$

The coefficients C_{nm} and S_{nm} describe the nature of the gravity field. For a perfect sphere, these coefficients all vanish. In the case of the Earth, the coefficient C_{20} has a value of -1083×10^{-6} due to the rotational oblateness, while all the other coefficients have values of the order of 1×10^{-6} or less. For the Moon, the values of C_{20} is also dominant, but is only about -200×10^{-6}, one fifth that for the Earth. As seen in the results of the Selenodesy work (cf. Table II), some of the other coefficients can also be significantly large.

* These equations are singular for $e=0$ and for $\sin\,i=0$. A modified set for small i using the elements $p=\tan i\sin\Omega$, $q=\tan i\cos\Omega$, $\tilde{\omega}=\omega+\Omega$ has been programmed, and a parallel set for small values of $\pi-i$. The small eccentricity case is not treated separately.

Whether the spherical harmonic expansion is the best means of representing the Moon's gravity has been brought into question by some of the recent studies. The problem arises only in regard to close orbiters, since their motion is affected by surface gravity anomalies that could not be noticed at greater distances. For this case, a model including a distribution of point masses on the lunar surface has met with some success. However, the results reported herein are all based on spherical harmonics.

To apply the method of averages, it is first necessary to represent the gravity potential as a function of position in orbit elements rather than in spherical coordinates. The general formulation is quite complicated, and will not be reproduced here. Some of the individual terms, however, are interesting in themselves, and as examples of the contribution of gravity harmonics to the changes in the spacecraft orbit.

The rates of the mean Keplerian elements due to C_{20} are

$$\frac{\mathrm{d}a}{\mathrm{d}t} = \frac{\mathrm{d}e}{\mathrm{d}t} = \frac{\mathrm{d}i}{\mathrm{d}t} = 0, \tag{15}$$

$$\frac{\mathrm{d}\Omega}{\mathrm{d}t} = \frac{3}{2}\frac{n\cos i}{p^2} C_{20}, \tag{16}$$

$$\frac{\mathrm{d}\omega}{\mathrm{d}t} = \frac{3n(1-5\cos^2 i)}{4p^2} C_{20}. \tag{17}$$

Those due to C_{22} and S_{22} are

$$\frac{\mathrm{d}a}{\mathrm{d}t} = \frac{\mathrm{d}e}{\mathrm{d}t} = 0, \tag{18}$$

$$\frac{\mathrm{d}i}{\mathrm{d}t} = \frac{3n\sin i}{p^2}\left[C_{22}\sin 2(\Omega-\theta) + S_{22}\sin 2(\Omega-\theta)\right], \tag{19}$$

$$\frac{\mathrm{d}\Omega}{\mathrm{d}t} = \frac{3n\cos i}{p^2}\left[C_{22}\cos 2(\Omega-\theta) + S_{22}\sin 2(\Omega-\theta)\right], \tag{20}$$

$$\frac{\mathrm{d}\omega}{\mathrm{d}t} = \frac{3n(3-5\cos^2 i)}{2p^2}\left[C_{22}\cos 2(\Omega-\theta) + S_{22}\sin 2(\Omega-\theta)\right]. \tag{21}$$

Those due to C_{30} are

$$\frac{\mathrm{d}a}{\mathrm{d}t} = 0, \tag{22}$$

$$\frac{\mathrm{d}e}{\mathrm{d}t} = \frac{3n\cos\omega}{2p^3}(1-e^2)\sin i\left(\tfrac{5}{4}\sin^2 i - 1\right), \tag{23}$$

$$\frac{\mathrm{d}i}{\mathrm{d}t} = \frac{3ne}{2p^3}\cos\omega\cos i\left(\tfrac{5}{4}\sin^2 i - 1\right), \tag{24}$$

$$\frac{\mathrm{d}\Omega}{\mathrm{d}t} = \frac{3ne}{2p^3}\sin\omega\cot i\left(\tfrac{15}{4}\sin^2 i - 1\right), \tag{25}$$

$$\frac{d\omega}{dt} = \frac{3n \sin \omega}{2p^3} \left(\frac{1 + 4e^2}{e} \sin i - e \cot i \right) \times \left(\tfrac{15}{4} \sin^2 i - 1 \right). \tag{26}$$

It is seen that the mean semimajor axis is not affected by any of the harmonics, and this is true in general. Only non-gravitational forces such as drag and radiation pressure affect the mean semimajor axis. Eccentricity is not affected by the second degree harmonics. The main cause for changes in eccentricity are the odd-degree harmonics, and also third body effects, e.g., Earth and Sun.

Inclination is not affected by C_{20}, the largest harmonic. Each of the other harmonics contributes to changes in i. However, all such contributions are periodic, with the period of either Ω or ω (or multiples thereof).

Node and omega are perturbed by all the harmonics, with secular contributions from the even zonals.

D. RADIATION PRESSURE

Rates of the averaged elements due to radiation pressure are computed by the formulas derived in [22]. Shadowing is accounted for, as described in [23]. Only the one component of radiation pressure, namely that along the spacecraft-sun line is included.

5. Numerical Analysis

A. FITTING THE NORMAL POINTS

The mechanics of fitting the normal points are described in this section. The computations were effected with the selenodesy program system based on the model described in Section 4, programmed by Dale Boggs (cf. [21]).

The first set of normal points was generated using the LaRC Sept. 11 harmonic model (since at the time it represented the best available) and an *a priori* radiation constant of 1.2111×10^{-10} km/s^2. This led to JPL mod-1 (cf. Table II) by fitting to arcs IB, IIC, IIIB, IVA, and IVC.

New normal points were generated with the mod-1 harmonics. These points were fit to both the 8–4 set of harmonics and radiation pressure, yielding JPL mod-2 with the high value for radiation pressure of 3.2897×10^{-10} km/s^2. Arcs IA, IB, IIC, IIIB, IIIC, IIIE, IVC, VC, and VD were used.

Arc IVA, the only high orbit, was not used because photomaneuvers occurring throughout this orbit had seriously perturbed the orbit, degrading its usefulness for gravity analysis. The principal evidence of this effect is the drift of 1 km in semimajor axis over 1 mo, which cannot be accounted for by gravity or radiation pressure. Again, new normal points were computed.

Before generating mod-3, the points of each arc were evaluated separately for maverick points, for biased stretches of data, for consistency with the initial state, and for consistency with the value of the radiation pressure constant. The result was a culling of points from arcs IB and IIIB particularly. Also, the initial values of the state and of radiation pressure for each arc were estimated. This had to be done as a separate operation because the selenodesy program system is limited to 50 parameters in any estimation. The resulting changes in the initial state are generally small. Those that were significant are listed in Table X.

Radiation pressure required special treatment. From engineering considerations, it is estimated that the acceleration along the sun-probe line due to solar pressure is 1.211×10^{-10} km/s^{-2}. However, solar pressure torque and gravity gradient torque induced attitude jet impulses resulting in additional accelerations. In addition, sun acquisition after each solar occultation required jet action; attitude bias for thermal control required jet action, and also changed the configuration relative to the torque producing forces; and attitude maneuvers for other engineering reasons resulted in jet action. The net effect was complicated and costly to model. A compromise method of attack was therefore adopted, in which an effective value for radiation pressure was estimated from the data for each arc of each orbiter.

The last column of Table X shows the radiation pressure constants actually used in the fit to the normal points. It was found that some arcs, specifically the high inclination arcs IVC, VC, and VD, the low eccentricity arc IIIE and arc IID were so insensitive to radiation pressure as not to yield a reliable value of the constant. The *a priori* engineering value was used for these arcs.

The fit to the data obtained for mod-3 was disappointing when measured by the quality of the data itself. On the residual graphs* (Figure 6), it is seen that there remains an appreciable bias in each of the Keplerian elements, but most strongly in eccentricity.

Table IX summarizes the quality of the fit to each of the twelve arcs. The average residuals listed are a measure of the secular bias of the data, since the initial residuals (residuals at the first point of the arc) are generally small. The standard deviations are a measure of the scatter in the data, although affected also by the bias.

It is difficult to see any pattern in these results. As might be expected, of course, the shorter arcs and the arcs with more points exhibit better fits. Also, it should be noted that for the low inclination orbits, the parameter $\Omega + \omega$ fits the data better than either Ω or ω separately. The reason is apparent when it is noted that in the limit, as i tends to zero, the values of Ω and ω become indeterminate.

After the basic mod-3 was obtained, it was thought desirable to generate some alternate models based on the same set of normal points, or portions thereof in order to check the consistency of the model and the sensitivity of the fit to the model.

The first alternate model was generated using diagonal weighting matrices instead of the natural ones derived from the data. As was to be expected, the Ω and ω data was fit appreciably better at the expense of the eccentricity. The diagonal matrices do not account for the very high correlation between Ω and ω and hence over-weight them.

For the next case all the data but semimajor axis was used and only the zonals plus

* Only arc IIC is included in these figures. For the remaining arcs, residual plots are shown in [10].

S_{31} and C_{31} were estimated. The result was JPL mod-4 (Table II). For this and the succeeding models the value of C_{22} was based on Koziel's libration studies and the estimated value of C_{20} iteratively using Equation (5) of Section 2. It is interesting to note that the values of the harmonics compare reasonably with those of mod-3, and furthermore the residuals are not appreciably worse.

JPL mod-5 represents a fit to the eccentricity data only, and as such fits the eccen-

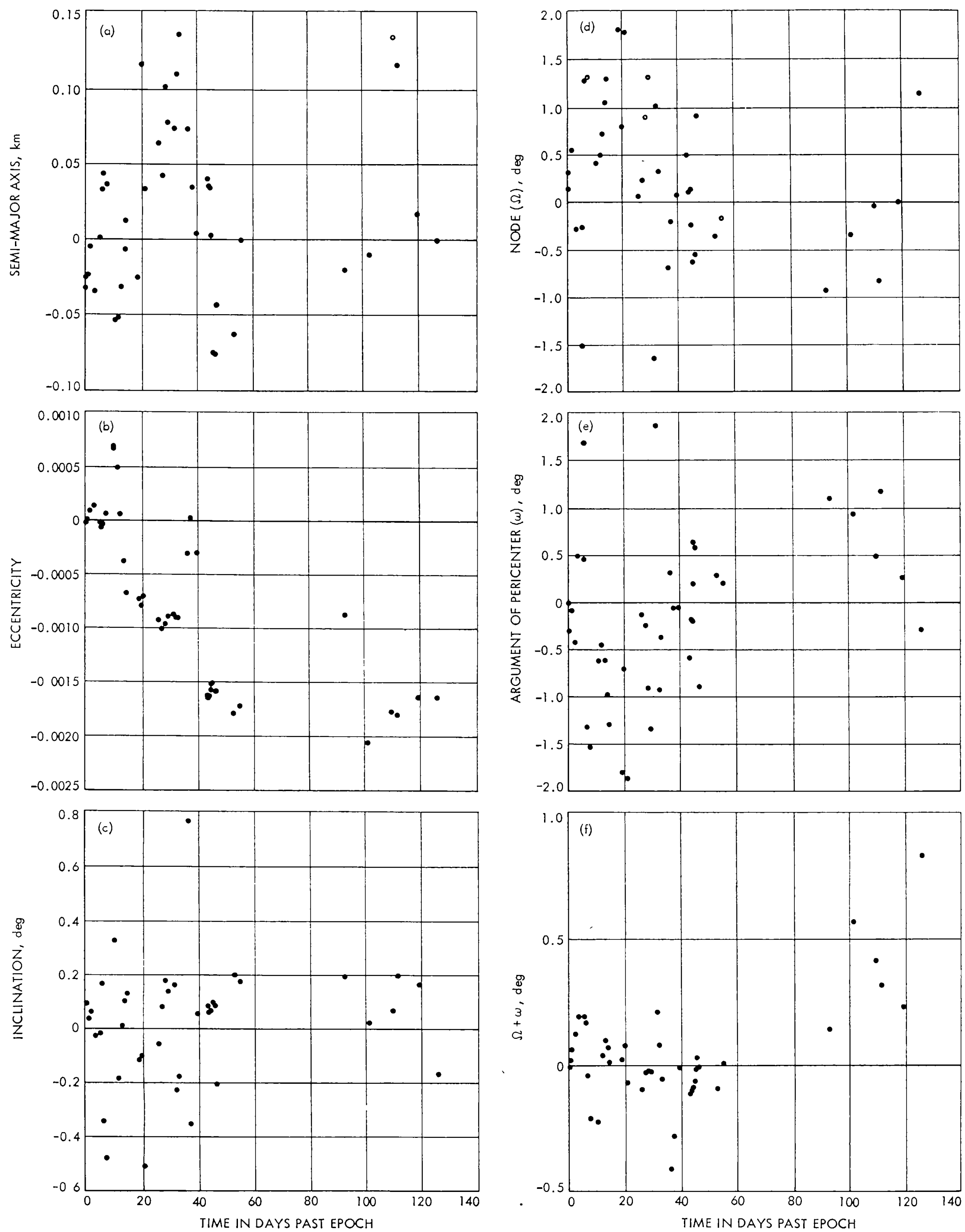

Fig. 6. Data residuals for JPL harmonic mod-3, arc IIC.

TABLE X

Changes in initial state and value of radiation pressure for each arc as determined by fitting the normal points

Arc	$a(m)$	e	i(deg)	Ω(deg)	ω(deg)	Solar radiation pressure (10^{-10} km^{2}s^{-2})
IA	−3	–	–	–	–	1.016
IB	+34	–	–	–	–	2.049
IIC	+25	–	–	–	–	0.942
IID	–	–	–	–	–	1.211[a]
IIE	−13	–	–	–	–	1.216
IIIB	−80	–	+0.30	+0.37	+0.32	1.712
IIIC	−18	–	–	–	–	2.097
IIID	–	–	–	–	–	1.184
IIIE	–	–	–	–	–	1.211[a]
IVC	–	–	–	–	–	1.211[a]
VC	−11	–	–	–	–	1.211[a]
VD	–	–	–	–	–	1.211[a]

[a] Solar pressure constant not estimated. The value 1.211×10^{-10} is an *a priori* engineering estimate.

tricity best. However, the fit to the other parameters deteriorates. The eccentricity data was also fit to all the harmonics (8–4 model, results not shown) yielding a much better fit to eccentricity, but a correspondingly poorer fit to the angle data.

JPL mod-6 is an extension of mod-4 to include C_{41} and S_{41}. Finally, mod-7 corresponds to mod-6 without the high inclination orbit data, orbits IVC, VC, and VD.

The experimentation with these several models leads to the following conclusions: (1) inclusion of tesserals through degree and order 4 is not effective in improving the model; thus, a zonal-only model (plus C_{22}, C_{31} and S_{31}, which are important) is almost as good as a complete 8–4 model; (2) selection of data types, e.g., fitting to eccentricity only, does not improve matters; and (3) the most complete model obtained (mod-3) fits the data to approx. 0.001 in eccentricity, 0.3° in inclination and 1.0° in Ω and ω.

The current work with mascons points to the reason for the poor showing of the 8–4 model. A recent calculation* in which a mascon represented by 15th degree harmonics was included with mod-3, improved the data fit for one arc by 90%. Thus, improvement of the model depends on going to higher degree and order, at least for close orbiters.

B. EVALUATION OF APOLLO-TYPE ORBIT (ARC IIIE)

The residual graphs and Table IX show that arc IIIE is fit more poorly than most of the other arcs. In particular, the secular trends in the residuals are very large. Node

* Reported by P. A. Laing of JPL.

TABLE XI

Partial derivatives, arc IIIE at 39 days

Parameter	$\partial e/\partial C$	$\partial i/\partial C$(deg)	$\partial \Omega/\partial C$(deg)	$\partial \omega/\partial C$(deg)	$\partial a/\partial C(m)$
C_{20}	26	−3982	165300	−277700	0
C_{40}	− 16	5922	−251900	378300	0
C_{60}	− 41	−4885	221700	−264800	0
C_{80}	84	577	− 55630	74370	0
C_{30}	804	−6490	− 5086	−120460	0
C_{50}	− 1122	9072	− 674	187550	0
C_{70}	836	−7130	11920	−155700	0
Radiation pressure	0.00049	0.002	− 0.007	− 0.071	−192 (per 10^{-10} km/s^2)

residuals increase 3.5° over the 40-day arc and ω residuals decrease 4.0°. The scatter in the data appears from the graphs to be about $\pm 1.0°$.

In Table XI the sensitivity of the IIIE orbit to the zonal harmonics and to radiation pressure is exhibited in order to see the magnitude change in zonal harmonics required to absorb the trend in the data. It is seen that values of the order of 10^{-5} for some of the zonals would be sufficient. Thus, IIIE is quite sensitive to the zonal harmonics, and thus to the whole gravity model. It stands to reason, then, that a truncated model (i.e., an 8–4 model) designed to fit all arcs, may do very poorly on IIIE.

In order to more nearly tailor the model to IIIE, the high-inclination orbits were omitted in fitting the data, leading to mod-7 (cf. Table III). The improvement of the data fit is shown in Table XII which compares the residual averages and standard deviations for mod-4 and mod-7.

On the basis of the averages, the improvement is marked, especially in eccentricity. Node and ω secular trends are reduced by better than a factor of 2. On the other hand the standard deviations are not changed appreciably. This reflects partly the fact that mod-7 is primarily a zonal model, and partly that the high-order harmonics are important.

TABLE XII

Residual statistics, arc IIIE

Parameter	Averages		Standard deviation	
	mod-7	mod-3	mod-7	mod-3
a(m)	41.8	41.9	72.2	58.0
$10^6\,e$	−84	−2514	2017	2061
i(deg)	−0.198	−0.024	0.266	0.217
Ω(deg)	0.879	2.074	1.066	1.053
ω(deg)	−0.946	−2.158	1.351	1.191
$\Omega+\omega$(deg)	−0.067	−0.084		

Radiation pressure cannot be estimated effectively from the IIIE data, an indication that attitude control system effects predominate in the semimajor axis data. This is an aggravating factor in producing the high residuals.

C. STATISTICS

The normal point estimates were obtained as differential corrections using a least-squares fit to the data (see [24], Equation (49)). Since the weighting matrix W depends on the *a priori* weighting of the Doppler data, it follows that the standard deviations of the harmonic coefficients obtained as the square roots of the diagonal terms in Γ must also depend on the Doppler weights. In fact, the two are proportional. Thus

$$\sigma_c = k\sigma_d,$$

in which k is a constant, σ_c represents a harmonic standard deviation and σ_d the

Doppler standard deviation. The implications have already been discussed in Section 3.C.

On the other hand, the correlations are independent of the Doppler statistics. Correlation matrices were obtained for each gravity model, that for mod-3 being exhibited in Table XIII. It is difficult to make value judgments on the basis of multivariate correlations, except to note that there are no very high correlations, i.e., values over 0.90. Furthermore, in spite of the non-linearity of the system, convergence occurred within a few iterations.

The difficulty arises primarily because the Moon is rough (gravitationally) and the orbiters were close in. A secondary source of the difficulty is the selective nature of the particular orbits, i.e., periselenium near equator, few inclinations, no far side data.

In spite of these problems, a long-arc analysis has been successfully accomplished, yielding an 8–4 gravity model (JPL mod-3). The data fit for this model suffers for the lack of high-order harmonics. However, it effectively fits the secular trends in the orbit element over all the data arcs, and it is reasonably compatible with the libration data and the results of Koziel.

Currently, the short-arc attack (mascon analysis) is attracting much attention. It should yield (in fact it already has) information on the surface structure of the Moon of considerable value in resolving long standing selenologic questions. However, the nature of the global structure, i.e., the low-degree gravity harmonics and moments of inertia, requires a long-arc approach.

Convergence to seven decimal places was obtained consistently, the eighth decimal place never quite settling down, suggesting a numerical precision to some seven decimals. Since most of the harmonics in the model have magnitude of order 10^{-4} or less, it follows that the results are good to about three significant digits – judged as a specified model fit to the given normal points.

6. Conclusions

Extraction of gravity information from Lunar Orbiter tracking data is a complicated and expensive operation.

A different approach based on short-arc analysis is allowing Sjogren* *et al.* to evaluate the fine structure of part of the Moon's gravity field. This method too has its difficulties due to indeterminacy of orbits, correlations between gravity harmonics and orbit parameters, and incompleteness of the model.

It is to be expected that the gravity information in the orbiter data will eventually all be extracted. The process of extracting it will no doubt involve a combination of methods, using both the short-arc and the long-arc methods.

In this connection there is a point where the two methods overlap, namely in the degree to which the mascons contribute to the global effects. For example, one might ask what fraction of C_{20} is due to mascons? In any case, the long-arc method must

* W. L. Sjogren, P. M. Muller, P. Gottlieb of JPL.

TABLE XIII

Correlation matrix for JPL mod-3

Run of MOPOS – SPS statistics link version 1 – May 1966
Correlation matrix with *a priori* sigmas on diagonal Label = 56

	C_{20} Column 1	S_{21} Column 2	C_{21} Column 3	S_{22} Column 4	C_{22} Column 5
C_{20}	9.92373236682D—11	1.85062510520D—02	2.13145259608D—01	—2.10334262666D—01	5.28148588417D—02
S_{21}	1.85062510520D—02	3.13556453387D—10	1.85206690823D—01	—8.80018300825D—03	3.83778824465D—02
C_{21}	2.13145259608D—01	1.85206690823D—01	3.91416684963D—10	7.39992483293D—02	6.37837401510D—02
S_{22}	—2.10334262666D—01	—8.80018300825D—03	7.39992483293D—02	2.69882974110D—10	—6.44278216684D—02
C_{22}	5.28148588417D—02	3.83778824465D—02	6.37837401510D—02	—6.44278216684D—02	2.83659241089D—10
C_{30}	—2.83276955362D—03	1.53649595572D—01	2.66435262595D—01	3.94690369048D—02	1.14748091812D—01
S_{31}	2.71204219853D—01	2.55482416245D—02	9.33015423024D—02	—2.22203486588D—01	—7.38843935286D—02
C_{31}	—1.51597178302D—04	—1.01135187813D—01	7.80059246722D—02	—1.05950814191D—01	3.47403547449D—02
S_{32}	1.64251529403D—01	—5.78642358834D—02	—1.32872149054D—01	—5.44616813109D—02	—2.28868339222D—01
C_{32}	4.39428348221D—02	—8.86251703444D—02	9.14813925701D—02	—9.03242697946D—03	—9.70977707022D—03
S_{33}	—3.01421263372D—02	2.54150327752D—02	2.47869673496D—01	1.52103342025D—02	3.09718849433D—01
C_{33}	2.31975088267D—01	—9.20301339490D—02	—9.99508820761D—02	—2.93582552432D—01	—9.81763620973D—02
C_{40}	4.06017431018D—01	—9.11782984069D—02	1.86248786062D—01	—1.11904797889D—01	9.72442028817D—02
S_{41}	8.42333568920D—02	7.58068081654D—01	1.01580437269D—01	—3.53652994394D—02	7.37971446828D—02
C_{41}	1.23518866908D—01	2.23195860665D—01	7.83635266926D—01	6.99016926903D—02	1.15018653501D—01
S_{42}	2.27995278372D—01	—1.54293208731D—02	—6.93532161469D—02	—2.15339819150D—01	1.17561716919D—01
C_{42}	1.06596668037D—01	1.30807081969D—01	6.99816908248D—03	1.04073553094D—02	—1.72407357653D—01
S_{43}	2.71508509006D—01	3.77465716101D—02	2.62389312528D—01	—9.05146115360D—02	1.94617916203D—03
C_{43}	2.55188545501D—01	—3.27864669992D—02	4.99182151819D—01	5.85432638163D—02	1.23984534189D—01
S_{44}	—1.42152854212D—01	8.22541074329D—02	—1.15864707740D—01	2.83353634835D—02	3.36790054555D—01
C_{44}	—1.16301170562D—01	—1.35526599512D—02	2.30145641173D—02	1.02222575693D—01	—5.88114950682D—02
C_{50}	—2.01521960976D—01	—4.13855743992D—02	—2.80626134562D—01	—1.32814464585D—02	—5.29259598284D—02
C_{60}	—5.65677446744D—01	—1.50923193858D—01	—7.55838469099D—02	5.71751251236D—02	2.91062769920D—02
C_{70}	—1.72619758241D—01	—1.17015004400D—01	—3.38571040111D—01	—1.74672861100D—02	—9.63429868069D—02
C_{80}	—5.62244942157D—01	—1.66778323765D—01	—6.57235173355D—02	5.46714744058D—02	1.12034657219D—01

Table XIII (continued)

Run of MOPOS – SPS statistics link version 1 – May 1966
Correlation matrix with *a priori* sigmas on diagonal Label = 56

	C_{30} Column 6	S_{31} Column 7	C_{31} Column 8	S_{32} Column 9	C_{32} Column 10
C_{20}	—2.83276955362D—03	2.71204219853D—01	—1.51597178302D—04	1.64251529403D—01	4.39428348221D—02
S_{21}	1.53649595572D—01	2.55482416245D—02	—1.01135187813D—01	—5.78642358834D—02	—8.86251703444D—02
C_{21}	2.66435262595D—01	9.33015423024D—02	7.80059246722D—02	—1.32872149054D—01	9.14813925701D—02
S_{22}	3.94690369048D—02	—2.22203486588D—01	—1.05950814191D—01	—5.44616813109D—02	—9.03242697946D—03
C_{22}	1.14748091812D—01	—7.38843935286D—02	3.47403547449D—02	—2.28868339222D—01	—9.70977707022D—03
C_{30}	1.71640747139D—10	2.20045738196D—02	1.63510631317D—02	—5.13423114135D—02	3.49271131741D—02
S_{31}	2.20045738196D—02	3.97191007140D—11	1.94329957620D—01	2.16323629819D—02	5.53270905063D—02
C_{31}	1.63510631317D—02	1.94329957620D—01	3.79708903694D—11	4.97006019358D—01	3.20937317849D—01
S_{32}	—5.13423114135D—02	2.16323629819D—02	4.97006019358D—01	4.03536609301D—11	3.89565009796D—01
C_{32}	3.49271131741D—02	5.53270905063D—02	3.20937317849D—01	3.89565009796D—01	4.31156254199D—11
S_{33}	1.97009521335D—01	—1.63600733111D—01	1.19163857203D—01	—1.28218692812D—01	1.29099817616D—01
C_{33}	—7.15241052842D—02	3.13264958244D—01	1.70320537071D—01	2.61525354974D—02	2.59507268265D—01
C_{40}	—2.45555416876D—01	1.03885994266D—01	7.30160978517D—02	—7.19227469213D—02	1.57954809361D—01
S_{41}	2.00154255336D—01	1.27230472489D—01	—1.42732813524D—01	9.16662028829D—02	1.45660660942D—01
C_{41}	2.28000977492D—01	1.56093490311D—01	—3.19684988149D—02	—1.92595713422D—01	9.32416763237D—02
S_{42}	4.18681617970D—02	2.91249065960D—02	1.38111282314D—01	3.24717311159D—02	—2.01241896823D—01
C_{42}	—8.13586115287D—02	—1.96831995418D—02	—1.09876893671D—01	3.71097551052D—01	—9.87134556539D—02
S_{43}	2.46548983614D—02	1.78077351102D—01	1.00953909331D—01	5.89420403226D—02	6.06725996993D—02
C_{43}	1.62395312307D—01	—4.47861552956D—02	—1.84540060074D—01	—2.41606914199D—01	2.57820845136D—02
S_{44}	3.74606121415D—02	5.77733298217D—02	3.33354442248D—02	2.04819277047D—02	5.46688649479D—02
C_{44}	8.22490943424D—02	—1.02386939080D—01	—1.11022321569D—01	1.36930759367D—02	—1.34761349801D—01
C_{50}	9.64078309712D—02	—2.31535484400D—02	—1.17266948953D—01	3.30232133350D—02	—2.51694372433D—03
C_{60}	—3.72279741980D—01	—1.50694855253D—01	4.67655227687D—02	—2.01053128061D—01	2.95506163047D—02
C_{70}	—5.23917629754D—01	—3.74408194896D—02	—1.36499331479D—01	1.83637503498D—02	—4.44686395523D—02
C_{80}	—1.84323271281D—01	—1.18081599980D—01	2.44528548277D—02	—2.93378569100D—01	—1.86875604607D—02

Table XIII (continued)

Run of MOPOS – SPS statistics link version 1 – May 1966
Correlation matrix with *a priori* sigmas on digital Label = 56

	S_{33} Column 11	C_{33} Column 12	C_{40} Column 13	S_{41} Column 14	C_{41} Column 15
C_{20}	—3.01421263372D—02	2.31975088267D—01	4.06017431018D—01	8.42333568920D—02	1.23518866908D—01
S_{21}	2.54150327752D—02	—9.20301339490D—02	—9.11782984069D—02	7.58068081654D—01	2.23195860665D—01
C_{21}	2.47869673496D—01	—9.99508820761D—02	1.86248786062D—01	1.01580437269D—01	7.83635266926D—01
S_{22}	1.52103342025D—02	—2.93582552432D—01	—1.11904797889D—01	—3.53652994394D—02	6.99016926903D—02
C_{22}	3.09718849433D—01	—9.81763620973D—02	9.72442028817D—02	7.37971446828D—02	1.15018653501D—01
C_{30}	1.97009521335D—01	—7.15241052842D—02	—2.45555416876D—01	2.00154255336D—01	2.28000977492D—01
S_{31}	—1.63600733111D—01	3.13264958244D—01	1.03885994266D—01	1.27230472489D—01	1.56093490311D—01
C_{31}	1.19163857203D—01	1.70320537071D—01	7.30160978517D—02	—1.42732813524D—01	—3.19684988149D—02
S_{32}	—1.28218692812D—01	2.61525354974D—02	—7.19227469213D—02	9.16662028829D—02	—1.92595713422D—01
C_{32}	1.29099817616D—01	2.59507268265D—01	1.57954809361D—01	1.45660660942D—01	9.32416763237D—02
S_{33}	6.17890894576D—11	—4.21511337189D—03	—1.12813449003D—01	1.26445288261D—01	1.78734339900D—01
C_{33}	—4.21511337189D—03	7.55578432411D—11	3.62772354872D—01	4.92281715434D—02	—7.64071886658D—02
C_{40}	—1.12813449003D—01	3.62772354872D—01	8.84598104700D—11	—2.68700711762D—03	2.04148957690D—01
S_{41}	1.26445288261D—01	4.92281715434D—02	—2.68700711762D—03	1.03232895389D—10	2.42798533582D—01
C_{41}	1.78734339900D—01	—7.64071886658D—02	2.04148957690D—01	2.42798533582D—01	1.16697397932D—10
S_{42}	—2.89905360826D—03	2.51695778061D—02	—7.88033060376D—02	—9.49451380435D—03	—1.53544062760D—02
C_{42}	—7.47937149435D—02	—6.73575243711D—02	—5.29921139914D—02	3.33125605711D—02	—9.28537628397D—02
S_{43}	—7.76409872768D—02	—2.03786280706D—01	—4.33227345273D—02	2.54651844256D—02	1.18719030767D—01
C_{43}	4.26357588300D—01	9.14711479338D—02	2.46694340375D—01	5.51770337671D—02	3.54396220518D—01
S_{44}	—6.38993411562D—03	1.57772413262D—01	—2.21424122783D—01	1.11672100778D—01	—9.66078329634D—02
C_{44}	—1.94304048283D—01	—3.85019159338D—01	—1.75641141908D—01	—8.98496008470D—02	2.54533549199D—02
C_{50}	—6.74879430160D—02	6.57181049315D—02	—2.23389921191D—01	—2.19275396711D—02	—1.93901513652D—01
C_{60}	—5.86430896316D—02	1.30734293513D—01	3.85261769037D—01	—1.90670471254D—01	—2.35717310178D—02
C_{70}	—1.49482994093D—01	9.52210176130D—02	—4.22788563728D—02	—1.54275066145D—01	—2.59598145605D—01
C_{80}	—2.41214914451D—02	7.11345212186D—02	2.44893346412D—01	—1.69101389138D—01	4.22693010901D—02

Table XIII (continued)

Run of MOPOS – SPS statistics link version 1 – May 1966
Correlation matrix with *a priori* sigmas on diagonal Label = 56

	S_{42} Column 16	C_{42} Column 17	S_{43} Column 18	C_{43} Column 19	S_{44} Column 20
C_{20}	2.27995278372D—01	1.06596668037D—01	2.71508509006D—01	2.55188545501D—01	—1.42152854212D—01
S_{21}	—1.54293208731D—02	1.30807081969D—01	3.77465716101D—02	—3.27864669993D—02	8.22541074329D—02
C_{21}	—6.93532161469D—02	6.99816908248D—03	2.62389312528D—01	4.99182151819D—01	—1.15864707740D—01
S_{22}	—2.15339819150D—01	1.04073553094D—02	—9.05146115360D—02	5.85432638163D—02	2.83353634835D—02
C_{22}	1.17561716919D—01	—1.72407357653D—01	1.94617916203D—03	1.23984534189D—01	3.36790054555D—01
C_{30}	4.18681617970D—02	—8.13586115287D—02	2.46548983614D—02	1.62395312307D—01	3.74606121415D—02
S_{31}	2.91249065960D—01	—1.96831995418D—02	1.78077351102D—01	—4.47861552956D—02	5.77733298217D—02
C_{31}	1.38111282314D—01	—1.09876893671D—01	1.00953909331D—01	—1.84540060074D—01	3.33354442248D—02
S_{32}	3.24717311159D—02	3.71097551052D—01	5.89420403226D—02	—2.41606914199D—01	2.04819277047D—02
C_{32}	—2.01241896823D—01	—9.87134556539D—02	6.06725996993D—02	2.57820845136D—02	5.46688649479D—02
S_{33}	—2.89905360826D—03	—7.47937149435D—02	—7.76409872768D—02	4.26357588300D—01	—6.38993411562D—03
C_{33}	2.51695778061D—02	—6.73575243711D—02	—2.03786280706D—01	9.14711479338D—02	1.57772413262D—01
C_{40}	—7.88033060376D—02	—5.29921139914D—02	—4.33227345273D—02	2.46694340375D—01	—2.21424122783D—01
S_{41}	—9.49451380435D—03	3.33125605711D—02	2.54651844256D—02	5.51770337671D—02	1.11672100778D—01
C_{41}	—1.53544062760D—02	—9.28537628397D—02	1.18719030767D—01	3.54396220518D—01	—9.66078329634D—02
S_{42}	5.90860911812D—11	—2.04136171972D—01	2.43037324000D—01	—5.35158476701D—02	1.41460881670D—03
C_{42}	—2.04136171972D—01	4.67397602710D—11	7.81812708166D—02	—1.68674106572D—01	7.35942371566D—02
S_{43}	2.43037324000D—01	7.81812708166D—02	4.17035466192D—11	—7.77186609801D—02	—3.46691240923D—02
C_{43}	—5.35158476701D—02	—1.68674106572D—01	—7.77186609801D—02	4.65431780947D—11	—7.15608427666D—02
S_{44}	1.41460881670D—03	7.35942371566D—02	—3.46691240923D—02	—7.15608427666D—02	1.14127989624D—11
C_{44}	—1.26200064014D—03	5.93815583467D—03	—3.61901424763D—02	—8.87465662854D—02	—8.57285000558D—02
C_{50}	6.07542630348D—02	7.60580061271D—02	—5.81521993443D—02	—6.92553818357D—02	3.02519722486D—02
C_{60}	—2.31299576299D—01	—1.40979436060D—01	—3.01980051306D—01	—2.12474906148D—02	—5.85080743611D—02
C_{70}	—3.46145050894D—03	9.08457551590D—02	—6.40989910650D—02	—1.17610844985D—01	—1.16638012956D—02
C_{80}	—1.28656825301D—01	—3.07762471742D—01	—2.92058799624D—01	—4.74652955199D—02	—3.18069528437D—02

Table XIII (continued)

Run of MOPOS – SPS statistics link version 1 – May 1966
Correlation matrix with *a priori* sigmas on diagonal Label = 56

	C_{44} Column 21	C_{50} Column 22	C_{60} Column 23	C_{70} Column 24	C_{80} Column 25
C_{20}	—1.16301170562D—01	—2.01521960976D—01	—5.65677446744D—01	—1.72619758241D—01	—5.62244942157D—01
S_{21}	—1.35526599512D—02	—4.13855743992D—02	—1.50923193858D—01	—1.17015004400D—01	—1.66778323765D—01
C_{21}	2.30145641173D—02	—2.80626134562D—01	—7.55838469099D—02	—3.38571040111D—02	—6.57235173355D—02
S_{22}	1.02222575693D—01	—1.32814464585D—02	5.71751251236D—02	—1.74672861100D—02	5.46714744058D—02
C_{22}	—5.88114950682D—02	—5.29259598284D—02	2.91062769920D—02	—9.63429868069D—02	1.12034657219D—01
C_{30}	8.22490943424D—02	9.64078309712D—02	—3.72279741980D—01	—5.23917629754D—01	—1.84323271281D—01
S_{31}	—1.02386939080D—01	—2.31535484400D—02	—1.50694855253D—01	—3.74408194896D—02	—1.18081599980D—01
C_{31}	—1.11022321569D—01	—1.17266948953D—01	4.67655227687D—02	—1.36499331479D—01	2.44528548277D—02
S_{32}	1.36930759367D—02	3.30232133350D—02	—2.01053128061D—01	1.83637503498D—02	—2.93378569100D—01
C_{32}	—1.34761349801D—01	—2.51694372433D—03	2.95506163047D—02	—4.44686395523D—02	—1.86875604607D—02
S_{33}	—1.94304048283D—01	—6.74879430160D—02	—5.86430896316D—02	—1.49482994093D—01	—2.41214914451D—02
C_{33}	—3.85019159338D—01	6.57181049315D—02	1.30734293513D—01	9.52210176130D—02	7.11345212186D—02
C_{40}	—1.75641141908D—01	—2.23389921191D—01	3.85261769037D—01	—4.22788563728D—02	2.44893346412D—01
S_{41}	—8.98496008470D—02	—2.19275396711D—02	—1.90670471254D—01	—1.54275066145D—01	—1.69101389138D—01
C_{41}	2.54533549199D—02	—1.93901513652D—01	—2.35717310178D—02	—2.59598145605D—01	4.22693010901D—02
S_{42}	—1.26200064014D—03	6.07542630348D—02	—2.31299576299D—01	—3.46145050894D—03	—1.28656825301D—01
C_{42}	5.93815583467D—03	7.60580061271D—02	—1.40979436080D—01	9.08457551590D—02	—3.07762471742D—01
S_{43}	—3.61901424763D—02	—5.81521993443D—02	—3.01980051306D—01	—6.40989910650D—02	—2.92058799624D—01
C_{43}	—8.87465662854D—02	—6.92553818357D—02	—2.12474906148D—02	—1.17610844985D—01	—4.74652955199D—02
S_{44}	—8.57285000558D—02	3.02519722486D—02	—5.85080743611D—02	—1.16638012956D—02	—3.18069528437D—02
C_{44}	1.24308797883D—11	8.14206841663D—02	—5.55331060993D—02	1.39392502004D—02	—2.62586302394D—02
C_{50}	8.14206841663D—02	1.66881810705D—10	6.56151539805D—02	7.56941914705D—01	—8.45229855188D—02
C_{60}	—5.55331060993D—02	6.56151539805D—02	2.55477699405D—10	3.66676669588D—01	8.96267951967D—01
C_{70}	1.39392502004D—02	7.56941914705D—01	3.66676669588D—01	2.11382556162D—10	1.58568587908D—01
C_{80}	—2.62586302394D—02	—8.45229855188D—02	8.96267951967D—01	1.58568587908D—01	2.49841189800D—10

pick up the entire global effect, whereas the mascon approach only incompletely evaluates global structure.

Nomenclature

Mass distribution:

A, B, C = moments of inertia in ascending magnitude
α, β, γ, f = moment of inertia ratios; see Equation (2)
M = mass of Moon
R = radius of Moon
$g = 2C/2MR^2$
$\mu = GM_{☾}$
G = universal gravity constant

Gravity field:

Φ = potential; see Equation (14)
U = disturbing function
$P_n^m(z)$ = associated Legendre function of degree n, order m
C_{ij}, S_{ij} = harmonic coefficients; see Equation (14)

Coordinates:

ϕ, λ = latitude and longitude (with respect to ecliptic and equinox of 1950)
$a, e, i, \Omega, \omega, \chi$ = Kepler elements (see [18], p. 288 in which σ replaces χ)
$p = \tan i \sin \Omega$
$q = \tan i \cos \Omega$
$\tilde{\omega} = \Omega + \omega$

Acknowledgments

This paper presents the results of one phase of research carried out at the Jet Propulsion Laboratory, California Institute of Technology, under Contract No. NAS 7-100, sponsored by the National Aeronautics and Space Administration. Special credit must be given to Wm. Sjogren whose support in the data reduction and orbital data analysis was invaluable, to Phil Laing who implemented the normal point computation, and to Wm. Kaula of UCLA who acted as consultant.

References

[1] Lorell, J., Martin, W. L., and Sjogren, W. L.: 1967, 'Selenodesy Experiment', in *Supporting Research and Advanced Development*, Space Programs Summary 37–43, vol. IV, pp. 22–32. Jet Propulsion Laboratory, Pasadena, Calif.
[2] Akim, E. L.: 1967, 'Determination of the Gravitational Field of the Moon from the Motion of the Artificial Lunar Satellite Luna-10', *Sov. Phys. – Dokl.*, **2**, No. 10.
[3] Kopal, Z.: 1966, *An Introduction to the Study of the Moon*, D. Reidel, Holland.
[4] Jeffreys, H.: 1959, *The Earth*, Cambridge University Press, 4th ed.
[5] *The Measure of the Moon*, 1967 (ed. by Z. Kopal and C. L. Goudas), D. Reidel, Holland.

[6] Eckert, W. J.: 1965, 'On the Motions of the Perigee and Node and the Distribution of Mass in the Moon', *Astron. J.* **70**, 787–792.
[7] Lorell, J.: 1967, 'Magnitude of Second-Degree Harmonics in Lunar Gravity Field', in *Supporting Research and Advanced Development*, Space Programs Summary 37–45, vol. IV, Jet Propulsion Laboratory, Pasadena, Calif., pp. 13–16.
[8] Jeffreys, H.: 1961, 'On the Figure of the Moon', *Monthly Notices Roy. Astron. Soc.* **122**, 421–432.
[9] Muller, P. M. and Sjogren, W. L.: 1968, 'Mascons: Lunar Mass Concentrations', *Science* **165**, 680–684.
[10] Lorell, J. and Laing, P. A.: *Compilation of Lunar Orbiter Tracking Data Used for Long-Term Selenodesy*, Technical Memorandum 33-419. Jet Propulsion Laboratory, Pasadena, Calif., to be published.
[11] Lorell, J., Anderson, J. D., and Sjogren, W. L.: 1965, *Characteristics and Format of the Tracking Data to be Obtained by the NASA Deep Space Instrumentation Facility for Lunar Orbiter*, Technical Memorandum 33-230. Jet Propulsion Laboratory, Pasadena, Calif.
[12] Lorell, J. and Sjogren, W. L.: 1967, *Lunar Orbiter Data Analysis*, Technical Report 32-1220. Jet Propulsion Laboratory, Pasadena, Calif.
[13] Warner, M. R., Nead, M. W., and Hudson, R. H.: 1964, *The Orbit Determination Program of the Jet Propulsion Laboratory*, Technical Memorandum 33-168. Jet Propulsion Laboratory, Pasadena, Calif.
[14] Smart, W. M.: 1949, *Text Book on Spherical Astronomy*, 4th ed., Cambridge University Press.
[15] Lorell, J.: 1964, 'Orbit Determination for a Lunar Satellite', *J. Astronaut. Sci.* **9**, 1–7.
[16] Anderson, J. D. and Null, G. W.: 1963, 'The Evaluation of Certain Physical Constants from the Radio Tracking of Mariner II', AIAA paper no. 63–424, presented at the AIAA Astrodynamics Conference, Aug. 19–21, Yale University, New Haven, Conn.
[17] Null, G. W., Gordon, H. J., and Tito, D. A.: 1967, *The Mariner IV Flight Path and Its Determination From Tracking Data*, Technical Report 32-1108. Jet Propulsion Laboratory, Pasadena, Calif.
[18] Clemence, G. M. and Brouwer, D.: 1961, *Methods of Celestial Mechanics*, Academic Press, New York.
[19] Bogoliubov, N. N. and Mitropolsky, Y. A.: 1961, *Asymptotic Methods in the Theory of Non-Linear Oscillations* (transl. from the Russian). Hindustan Publishing Corp., New Delhi.
[20] Lorell, J., Anderson, J. D., and Lass, H.: 1964, *Application of the Method of Averages to Celestial Mechanics*, Technical Report 32-482. Jet Propulsion Laboratory, Pasadena, Calif.
[21] Boggs, D.: 1967, 'A Computer Program for the Determination of Some Coefficients of the Moon's Gravity Potential Expansion', in *Supporting Research and Advanced Development*, Space Programs Summary 37-47, vol. III, Jet Propulsion Laboratory, Pasadena, Calif., pp. 21–28.
[22] Bryant, R. W.: 'The Effect of Solar Radiation Pressure on the Motion of an Artificial Satellite', TN D-1063, NASA, Goddard Space Flight Center, Greenbelt, Md., Sept. 1961.
[23] Lorell, J.: 1968, 'Shadow Equation for a Satellite', in *Supporting Research and Advanced Development*, Space Programs Summary 37-51, vol. III, Jet Propulsion Laboratory, Pasadena, Calif., pp. 1–4.
[24] Anderson, J. D.: 1967, *Determination of the Masses of the Moon and Venus and the Astronomical Unit from Radio Tracking Data of the Mariner II Spacecraft*, Technical Report 32-816. Jet Propulsion Laboratory, Pasadena, Calif.
[25] Kaula, William M.: 1966, *Theory of Satellite Geodesy*, Blaisdell Pub. Co., Waltham, Mass.
[26] Tolson, R. H. and Gapcynski, J. P.: 1967, 'An Analysis of the Lunar Gravitational Field as Obtained from Lunar Orbiter Tracking Data', Paper presented at the IQSY/COSPAR Assemblies, London, England, July 17–28.